15 Energy Transfer to Multiple Acceptors in One, Two, or Three Dimensions

In the previous two chapters on energy transfer we considered primarily covalently linked donor–acceptor pairs, or situations in which there was a single acceptor near each donor. However, there are numerous situations in which there exist multiple acceptors, such as donors and acceptors dissolved in homogeneous solutions. More interesting examples of the multiple-acceptor case occur in membranes and nucleic acids. Suppose one has a lipid bilayer that contains both donors and acceptors (Figure 15.1). Each donor will be surrounded by acceptors in two dimensions. Since the acceptor distribution is random, each donor sees a different acceptor population. Hence, the intensity decay is an ensemble average and is typically non-exponential. A similar situation exists for donors and acceptors that are intercalated into double-helical DNA (Figure 15.1), except that in this case the acceptors are distributed in one-dimension along the DNA helix.

The theory for these multiple-acceptor cases is complex, even for random distributions in three dimensions. For a completely homogeneous and random solution, with no excluded volume, the form of the donor intensity decay and donor quantum yield is known, and was described by Förster.[1,2] However, consider a protein with a buried fluorophore that serves as the donor. The exact form of the intensity decay will depend on the acceptor concentration, and on the distance of closest approach (r_C) between the donor and acceptor, which could be approximated by the radius of the protein (Figure 15.1, left). The concept of a minimum D–A distance becomes particularly important for membrane-bound proteins, where r_C may reflect the size of a membrane-bound protein, the presence of boundary lipid which excludes the acceptor, or the distance of the donor above the membrane surface. The theory for resonance energy transfer (RET) under these conditions is complex. The theory becomes still more complex if we consider D–A diffusion. Hence, we cannot present a complete description of energy transfer for these diverse conditions. Instead we will present several examples. Additional references are presented in the section entitled "Additional References on RET between Unlinked Donor and Acceptor," after the main reference section.

15.1. RET IN THREE DIMENSIONS

The simplest example of RET to multiple acceptors is a homogeneous solution of donors and acceptors, without D–A diffusion. If the concentration of donor is adequately low so that there is no homotransfer between donors, the intensity decay is well known[1–3] and is given by

$$I_{DA}(t) = I_D^0 \exp\left[-\frac{t}{\tau_D} - 2\gamma\left(\frac{t}{\tau_D}\right)^{1/2} \right] \qquad (15.1)$$

where τ_D is the donor decay in the absence of acceptors. The term with the $\sqrt{t}$ time dependence is given by

$$\gamma = \frac{\Gamma(1/2)}{2}\frac{C}{C_0} \qquad (15.2)$$

In this expression $\Gamma(1/2) = \sqrt{\pi} = 1.7724539\ldots$ is the complete gamma function, C is the acceptor concentration, and C_0 is a characteristic acceptor concentration in molecules/cm^3. This concentration is related to the Förster distance by

$$C_0 = \left(\frac{4}{3}\pi R_0^3\right)^{-1} \qquad (15.3)$$

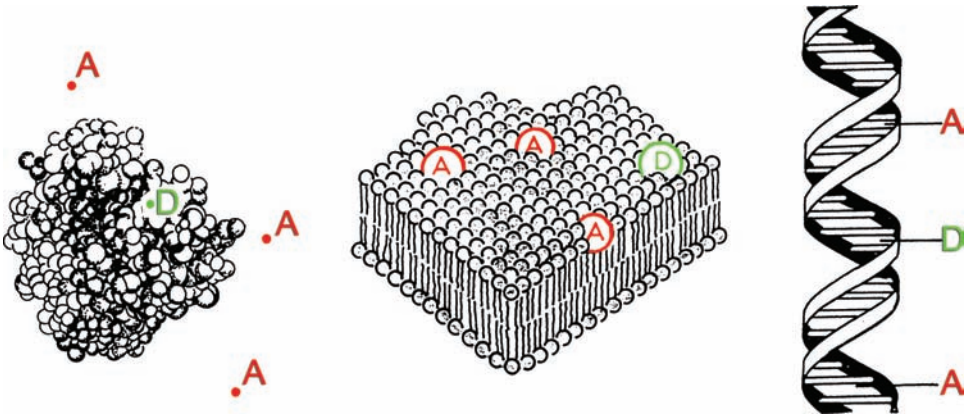

Figure 15.1. FRET between unlinked donors and acceptors in a protein (left), a lipid bilayer (middle), and in double-helical DNA (right).

The ratio C/C_0 is thus seen to be the number of acceptor molecules in a sphere of volume $4/3\pi R_0^3$.

For randomly distributed acceptors in three dimensions the steady-state intensity of the donor is given by

$$\frac{F_{DA}}{F_D} = 1 - \sqrt{\pi}\,\exp(\gamma^2)\left[1 - \mathrm{erf}(\gamma)\right] \qquad (15.4)$$

where the error function erf(γ) was defined in eq. 13.32. In contrast to a distance distribution between linked D–A pairs, we have an analytical expression like eqs. 15.1 and 15.4 for energy transfer between donors and acceptors dissolved in solution. An important consequence of unlinking the donors and acceptors is that the extent of transfer depends on acceptor concentration, and that the acceptor concentrations must be quite high for significant energy transfer. The acceptor concentration is often described in terms of C_0, which is the acceptor concentration needed for 72% transfer. The values of C_0 can be calculated from R_0, and are typically in the range 2–50 mM. This is the concentration of acceptors needed to statistically place an acceptor within a distance R_0 of the donor. The definition of C_0 is slightly related to A_0 in eq. 13.30 by $C_0 = 0.5\sqrt{\pi}A_0$. Both C_0 and A_0 are in common use.

The orientation factor κ^2 is not shown explicitly in eqs. 15.1–15.4, as a value of 2/3 is usually assumed during calculation of Förster distance R_0. In general, fluorophores rotate faster than they undergo translational diffusion. As a result it is often possible to find conditions where rotational motions result in dynamic averaging of κ^2 to 2/3. However, if the solution is completely frozen so that rotational motions are slower than the donor decay,[3–5] then for a random three-dimensional solution $\kappa^2 = 0.476$. Hence energy transfer is somewhat slower in rotationally frozen solutions compared to fluorophores that can rotate during the excited-state lifetime. To obtain the same energy transfer as with $\kappa^2 = 2/3$, the acceptor concentration needs to be 1.18-fold larger.[5]

15.1.1. Effect of Diffusion on FRET with Unlinked Donors and Acceptors

In Chapter 14 we described how D-to-A diffusion increases the efficiency of energy transfer between covalently linked D–A pairs. A similar effect occurs for unlinked D–A pairs in homogeneous solution. However, the theory for energy transfer for unlinked donors and acceptors becomes more complex in the presence of diffusion.[6–7] In fact, the theory has not been solved to yield exact analytical expressions to describe the intensity decay. Numerical solutions have been described,[7–8] but for purposes of least-squares data analysis it is usually more convenient to use approximate expressions that are available in a closed form. Several approximations are available. For unlinked donors and acceptors in homogeneous solution the donor decay can be described by[9]

$$I_{DA} = I_D^0 \exp\left[-\frac{t}{\tau_D} - 2B\gamma\left(\frac{t}{\tau_D}\right)^{1/2}\right] \qquad (15.5)$$

The parameter B is given by

$$B = \left(\frac{1 + 10.87x + 15.5x^2}{1 + 8.743x}\right)^{3/4} \qquad (15.6)$$

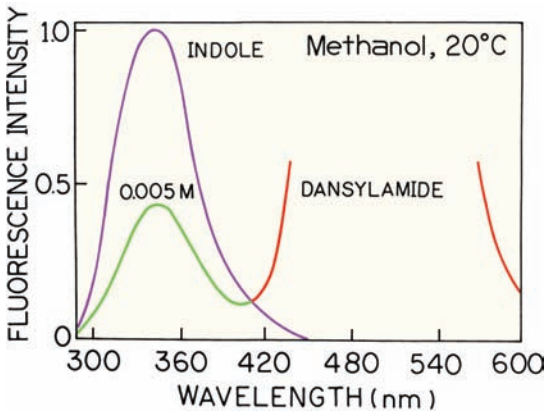

Figure 15.2. Emission spectra of an unlinked indole donor and 5 mM dansylamide acceptor in methanol at 20°C. Reprinted with permission from [13]. Copyright © 1990, American Chemical Society.

where

$$x = D\alpha^{-1/3}t^{2/3}, \quad \alpha = R_0^6/\tau_D \tag{15.7}$$

A second comparable expression is also available[10] where

$$B = \left(\frac{1 + 5.47x + 4.00x^2}{1 + 3.34x}\right)^{3/4} \tag{15.8}$$

It is claimed that this latter approximation is better for longer times.[10–11] If $D = 0$ these expressions become equivalent to eq. 15.1. These expressions are thought to be valid for a wide range of diffusion coefficients and acceptor concentrations.[12] The important point is that it is complex to exactly calculate the intensity decay in the presence of D–A diffusion, but the intensity decay can be predicted with good accuracy using the approximate expressions.

15.1.2. Experimental Studies of RET in Three Dimensions

There have been numerous studies of energy transfer in three-dimensional solution. It is generally accepted that eqs. 15.1–15.8 provide an accurate description for randomly distributed donors and acceptors.[6] To illustrate energy transfer in homogeneous solution we have chosen data for indole as the donor and dansylamide as the acceptor.[13] The donor and acceptor were dissolved in methanol, which is highly fluid, so that diffusion can be expected to increase the extent of energy transfer. In order to obtain significant energy transfer the dansyl amide concentration was 5 mM. The high acceptor concentrations needed for RET in solution between unlinked D–A pairs makes it difficult to measure the donor emission. This is seen from Figure 15.2, where the acceptor emission is much more intense than the donor emission. Of course the acceptor is excited both by energy transfer and by direct absorption. Careful optical filtering is needed to eliminate the acceptor emission, which is essential for measurement of the donor decay kinetics. Additionally, it is often necessary to use higher than usual concentrations of donor to obtain detectable donor emission in the presence of high acceptor concentrations and high optical densities. For these reasons, energy-transfer measurements in homogeneous solution are frequently performed using front-face observation. Even with front-face observation it is difficult and error prone to correct the donor intensities for the large inner filter effect. For this reason it is usually more convenient to use time-resolved measurements of the donor (Figure 15.3, solid curve), since the intensity decay is independent of the total intensity.

Examination of eq. 15.1 predicts that the donor intensity decay becomes non-exponential in the presence of dissolved acceptors. At the moment of excitation the solution contains donors that on average are surrounded by a constant concentration of acceptors at all distances. Some of the donors are located closer to acceptors than other donors. Following pulsed excitation these more closely spaced D–A pairs transfer rapidly, leading to a rapid component in the intensity decay, which is the $\sqrt{t}$ term in eq. 15.1. At longer times the decay becomes dominated by the

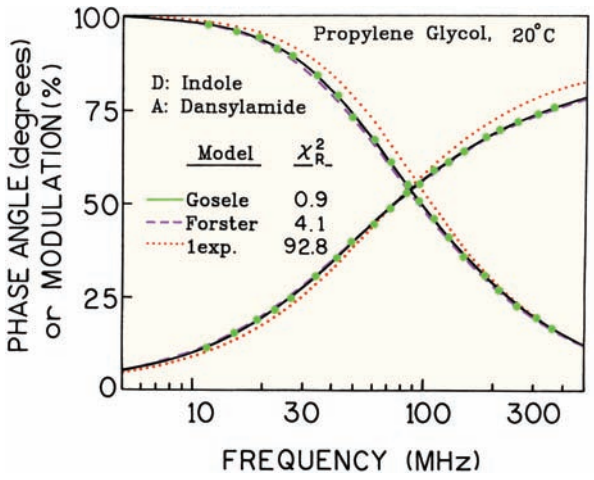

Figure 15.3. Frequency-domain intensity decays of indole with 12 mM dansylamide in propylene glycol at 20°C. Reprinted with permission from [13]. Copyright © 1990, American Chemical Society.

Table 15.1. Indole Decay Times and D-to-A Diffusion Coefficients in Propylene Glycol and Methanol at 20°C[a]

Solvent	[A]	eq. no.	τ_D (ns)	R_0 (Å)	10^6D (cm²/s)	χ_R^2
Propylene glycol	0	[b]	4.23			1.4
	12 mM	[b]	2.57			92.8
		15.1	<4.23>	24.9		4.1
		15.1	<4.23>	<24.3>[c]		10.6
		15.8	<4.23>	23.9	1.03	0.9
		15.8	<4.23>	<24.3>	0.62	1.3
Methanol	0	[b]	4.09			2.4
	5 mM	[b]	2.03			30.7
		15.1	<4.09>	37.1		95.8
		15.1	<4.09>	<26.1>		1152.1
		15.8	<4.09>	27.8	26.4	1.8
		15.8	<4.09>	<26.1>	34.0	3.1

[a]From [7]. The acceptor (A) was dansylamide.
[b]The data were fit to a single-exponential decay law.
[c]The angular brackets < > indicate that the parameter was held fixed during the analysis.

longer-lived donors, which are on average more distant from the acceptors.

In a fluid solvent like methanol the intensity decay of indole is influenced by translational diffusion that increases the extent of energy transfer. To understand the effects of diffusion it is useful to first consider the indole decay in the relatively viscous solvent propylene glycol, where little diffusion is expected during the 4.23-ns excited-state lifetime of indole. The donor decay from indole was examined using frequency-domain measurements (Figure 15.3). In the absence of acceptor the indole decay was a single exponential (Table 15.1). Because diffusion does not increase the transfer efficiency in this solvent, it was necessary to increase the acceptor concentration to 12 mM. In the presence of acceptor (12 mM dansylamide) the decay of indole can no longer be fit to a single decay time (dotted, χ_R^2 = 92.8). The donor intensity decay can better fit using eq. 15.1, resulting in a much improved value of χ_R^2 = 4.1. The variable parameter in this fit is C_0 or R_0. In fact, such measurements are a reliable means to experimentally determine R_0, assuming the acceptor concentration is known. In Figure 15.3 a still better fit was obtained using a model that accounts for D–A diffusion, because a small amount of D-to-A diffusion occurs in this solvent.

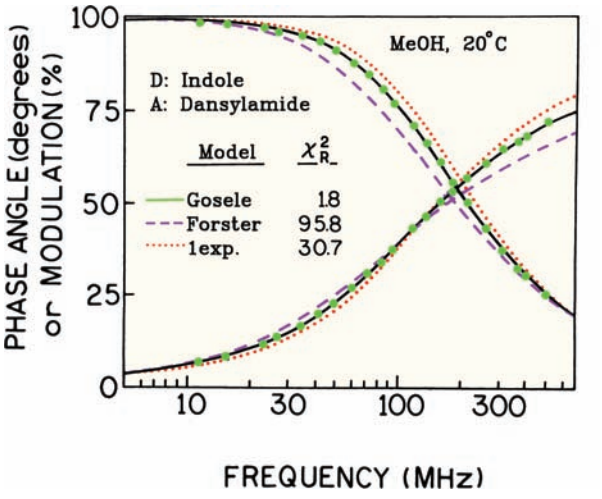

Figure 15.4. Frequency-domain donor decays of indole with 5 mM dansylamide in methanol at 20°C. Reprinted with permission from [13]. Copyright © 1990, American Chemical Society.

Figure 15.4 shows FD data for the indole–dansylamide DA pairs in methanol, which is less viscous than propylene glycol and allows significant diffusion during the donor's excited-state lifetime. In this case eq. 15.1 does not fit the data (Figure 15.4, dashed) because diffusion changes the shape of the intensity decay. The approximate expression for $I_{DA}(t)$ can be used to predict the donor intensity at any time, and thus used for analysis of FD and TD data. Diffusion results in a donor decay which is more like a single exponential, as can be seen by the deviations of the data (dot-dashed) from the Förster equation (dashed) toward the single-exponential model (dotted). The data were well fit by the approximate intensity decay described by eq. 15.8. The value of χ_R^2 = 95.8 obtained using the Förster model is artificially low because the fitting procedure increases R_0 to account for diffusion enhanced energy transfer. If the Förster distance is held constant at its known value at the

known value of 26.1 Å, then $\chi_R^2 = 1152$ (Table 15.1). This highly elevated χ_R^2 value indicates the significant influence of diffusion in this system. When the correct model is used (eq. 15.8) the variable parameters in the analysis are R_0 and the mutual diffusion coefficient D. Least-squares analysis yielded $R_0 = 27.8$ Å and $D = 2.64 \times 10^{-5}$ cm²/s (Table 15.1), which are reasonably close to the expected values in this solvent.

If the acceptor concentration is known the time-resolved data can be used to determine the Förster distance. In propylene glycol the recovered value of 24.9 Å is in good agreement with the calculated value of 24.3 Å. For the D–A pair in methanol it is interesting to consider the value of R_0 obtained if diffusion is neglected, which is accomplished by setting $D = 0$ during the least-squares analysis. In this case the apparent value of R_0 is larger, 37 Å. This result provides a useful hint. If the time-resolved data yield a larger than expected R_0 value, the cause could be diffusion during the donor excited-state lifetime. It should be noted that we have assumed that the distance of closest approach (r_C) is zero. If r_C is a significant fraction of R_0, then eqs. 15.1–15.8 are not appropriate.

The effect of diffusion on the donor intensity decay can be seen in the time-domain data. The impulse response functions for the indole–dansylamide mixtures are shown in Figure 15.5. It is visually evident that the dansyl acceptor results in a non-exponential indole decay in propylene glycol. In methanol the decay is still heterogeneous, but is closer to a single exponential. This trend towards a single-exponential donor decay in the presence of diffusion is well known in the literature,[14] and the donor decay becomes single exponential in the rapid diffusion limit (Section 15.6).

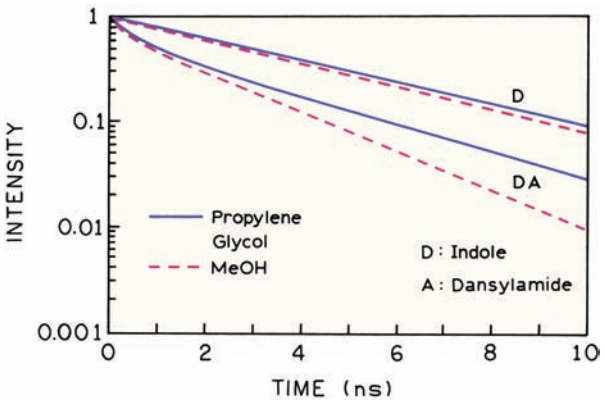

Figure 15.5. Reconstructed time-domain intensity decays of indole without acceptor (D) with 5 mM dansylamide in methanol (dashed) and with 12 mM dansylamide in propylene glycol (solid).

15.2. EFFECT OF DIMENSIONALITY ON RET

In the previous section we saw that a random distribution of an acceptor molecules around a donor resulted in a characteristic donor decay. For randomly distributed acceptors the form of the donor decay depends on the dimensionality of the acceptor distribution. Different donor decays are expected for acceptor distributions in a volume, in a plane, or along a line. Planar distributions are expected for donors and acceptors in membranes, and linear distribution are expected for dyes intercalated into double helical DNA (Figure 15.1). Assuming no diffusion, no excluded volume, and a random distribution of donors and acceptors in two dimensions or one dimension, the intensity decays are known in analytical form. For a random two-dimensional distribution,[15–16]

$$I_{DA}(t) = I_D^0 \exp\left[-\frac{t}{\tau_D} - 2\beta\left(\frac{t}{\tau_D}\right)^{1/3}\right] \qquad (15.9)$$

where

$$\beta = \frac{\Gamma(2/3)}{2}\frac{C}{C_0}, \qquad \Gamma(2/3) = 1.354177\ldots \qquad (15.10)$$

and

$$C_0 = (\pi R_0^2)^{-1} \qquad (15.11)$$

Hence C/C_0 is the number of acceptor molecules in an area equal to πR_0^2, that of a circle with diameter R_0.

For a random one-dimensional distribution of acceptors the donor intensity decay is given by

$$I_{DA}(t) = I_D^0 \exp\left[-\frac{t}{\tau_D} - 2\delta\left(\frac{t}{\tau_D}\right)^{1/6}\right] \qquad (15.12)$$

where

$$\delta = \frac{\Gamma(5/6)}{2}\frac{C}{C_0}, \quad \Gamma(5/6) = 1.128787\ldots \qquad (15.13)$$

and

$$C_0 = \frac{1}{2R_0} \qquad (15.14)$$

In this particular case the ratio C/C_0 is the number of acceptor molecules within a linear distance R_0 of the donor. For one-, two-, and three-dimensional distributions of acceptors there exist components that decay as $t^{1/6}$, $t^{1/3}$, and $t^{1/2}$, respectively. Values of the gamma function can be found from standard mathematical tables using $\Gamma(\alpha + 1) = \alpha\Gamma(\alpha)$. One may be interested in obtaining the relative quantum yields of the donor. While such expressions are available in one and two dimensions, these are infinite series and not closed-form expressions. With presently available computers and software it is equally easy to use numerical integration of eqs. 15.1, 15.9, and 15.12 to obtain the transfer donor efficiency. For $C = C_0$, where $\gamma = \beta = \delta = 1.0$, the energy transfer efficiencies are 72, 66, and 63%, respectively, in three, two, and one dimensions. A graph of the relative donor yields is given in Problem 15.3.

Prior to examining experimental data it is of interest to examine the forms of the donor decays. The effects of dimensionality on RET are shown using simulated data in Figure 15.6. For these simulations the acceptor concentrations were taken as equal to the values of C_0, which allowed the forms of intensity decays to be compared. As the dimensionality is reduced the time-domain intensity decays show an increased contribution of the short-time components, which are faster in one than in three dimensions. The difference in the intensity decay can also be seen in the frequency-domain simulations. These simulations suggest that the time-resolved decays can be used to determine the dimensionality of the system. In fact, analysis of the simulated frequency-domain data showed that the decay for one-dimensional RET could not be analyzed in terms of RET in two or three dimensions, and vice versa.[17–18] That is, the form of the intensity decays are unique in each dimension. In such studies the geometry of the system is often described as a combination of one, two, or three dimensions. Several groups have described the use of RET to determine the fractal dimensions of molecular surfaces.[19–21]

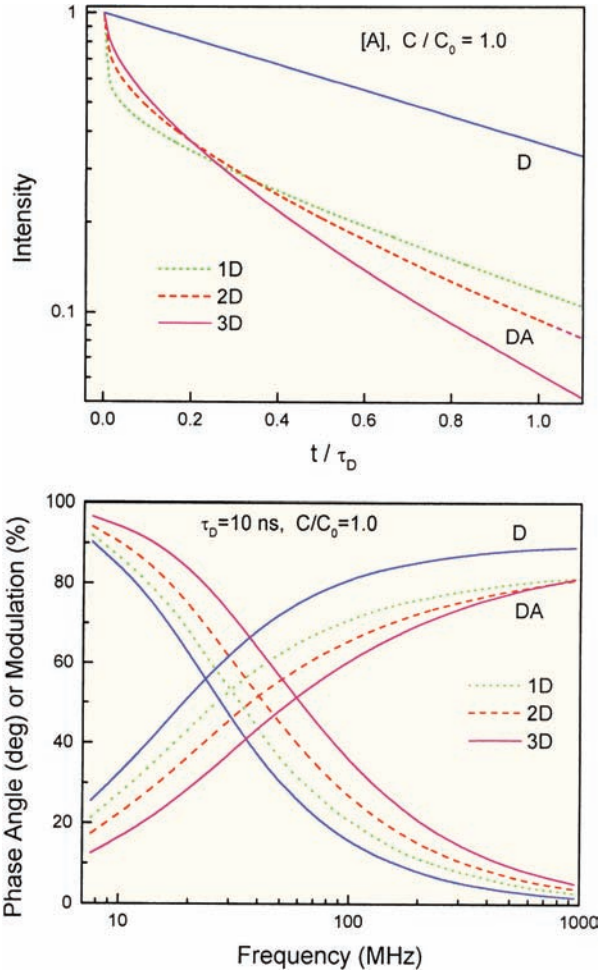

Figure 15.6. Effect of FRET in one-, two-, or three-dimension on the donor intensity decays. From [17].

15.2.1. Experimental FRET in Two Dimensions

In spite of the considerable interest in membrane organization, there have been relatively few time-resolved studies of RET in two dimensions. We will now describe two reports, one that confirmed the expected decay in two dimensions[22] (eq. 15.9) and one report that found more complex behavior.[23]

Energy transfer in two dimensions was examined using octadecyl rhodamine B (ORB) as the donor to a membrane-bound cyanine dye, $DiIC_1(7)$, which served as the acceptor (Figure 15.7). These dyes were dispersed in large unilamellar vesicles of dipalmitoylphosphatidylcholine (DPPC). The intensity decays of ORB became more rapid in vesicles containing increasing concentrations of the acceptor (Figure 15.7). When the temperature was above the lipid transition temperature the data were adequately fit to the two-dimensional intensity decay law. The data for temperatures above and below the phase-transition temperature were fit to a general expression:

$$I_{DA}(t) = \exp\left[-\frac{t}{\tau_D} - c\left(\frac{t}{\tau_D}\right)^{d/6}\right] \qquad (15.15)$$

where time-independent c is a constant[21] and d depends on dimensionality. The constant c is related to the surface den-

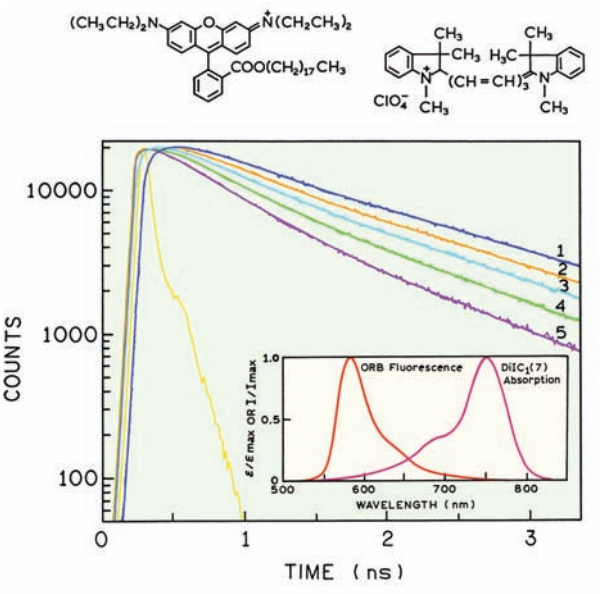

Figure 15.7. Time-domain intensity decay of ORB in DPPC at 50°C with $DiIC_1(7)$-to-DPPC ratios of 0 and 1 to 900, 450, 245, and 160, for numbers 1 to 5, respectively. Insert: ORB emission spectra and $DiIC_1(7)$ absorption spectrum. Revised from [22].

sity of the acceptors and the dimensionality of the systems.[24–25]

The time-resolved ORB donor decays (Figure 15.7) were used to recover the value of d in eq. 15.15. This was accomplished by least-squares analysis and examination of the χ_R^2 surfaces. For DPPC vesicles at 50°C, which is above the phase-transition temperature near 37°C, the value of d was near 2 and the donor decays were consistent with energy transfer in two dimensions ($t^{1/3}$ dependence). At 25°C, below the phase transition of the lipids, the time-resolved data were no longer consistent with 2D RET. In this case the value of d was found to be between 0.83 to 1.0, which is expected for energy transfer in one dimension ($t^{1/6}$). This effect was explained as co-localization of the donor and acceptor along defect lines in the bilayers. While one may argue with the exact interpretation of the results, it is clear that RET depends on the spatial distribution of donors and acceptors in the lipids. One can use the time-resolved decays to determine d in eq. 15.15, and thus the fractal dimension of the system. This has been accomplished for lipid bilayers,[26] and for dyes adsorbed to silica surfaces[27–29] and latex spheres.[30]

An important aspect of the analysis was measurements of both the steady-state donor intensities and the time-resolved decays. For the fluid-phase vesicles the intensities were well fit by theoretical data based on Monte Carlo simulations (Section 15.4). In contrast, for the gel-phase vesicles at 25°C the extent of donor quenching was greater than predicted for a random two-dimensional distribution (Figure 15.8). The direction of the deviations was toward the prediction for a one-dimensional system. This is what led the authors[22] to conclude that the donors and acceptors were co-localized around defect lines for the gel phase lipid. The important point of this comparison is that one can gain important insight by comparison of both the steady-state and time-resolved data. Such a comparison is a form of global analysis, in that multiple types of data are compared with a given molecular model.

For membrane-bound probes it is not always clear whether energy transfer is occurring in two or three dimen-

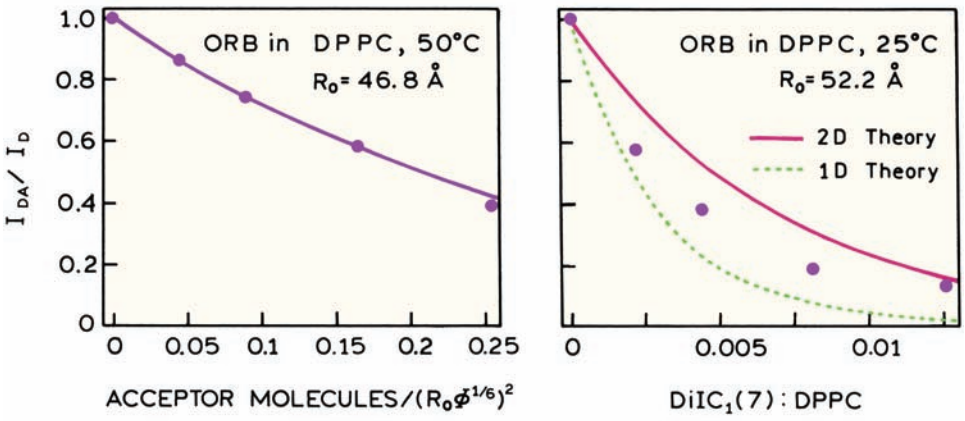

Figure 15.8. ORB donor intensities with increasing concentrations of $D_1IC_1(7)$ in DPPC vesicles at 50°C (left) and 25°C (right). Left: The line is for a two-dimensional model[48] with R_0 = 46.8 Å. ϕ is the donor quantum yield. Right: The solid and dashed lines are the theoretical predictions for RET in two and one dimensions with R_0 = 52.3 Å,[49] respectively. From [22].

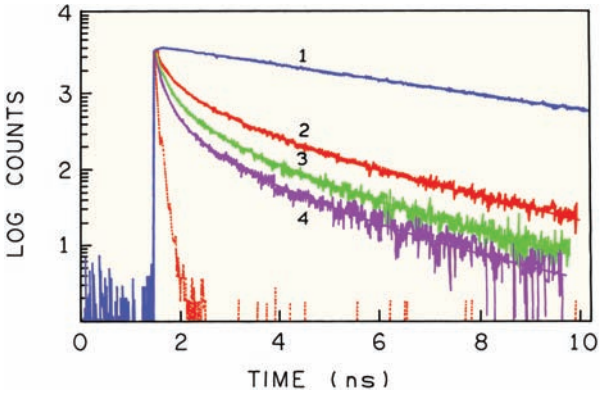

Figure 15.9. Rhodamine 6G donor decays absorbed to dihexadecyl phosphate vesicles. The acceptor was malachite green with concentrations of 0 M (1), 3.32 x 10^{-6} M (2), 4.40 x 10^{-6} M (3), and 5.27 x 10^{-6} M (4). Revised and reprinted with permission from [23]. Copyright © 1987, American Chemical Society.

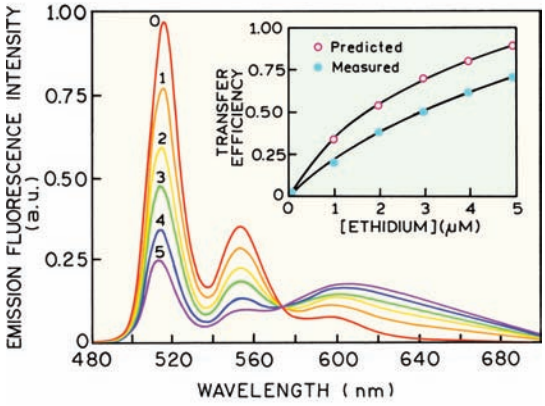

Figure 15.10. Emission spectra of dimethyldiazaperopyrenium bound to poly d(A-T) with increasing concentrations of ethidium bromide. The insert shows a comparison of the measured (●) and predicted (○) transfer efficiencies. Revised from [32].

sions. Energy transfer to surface-localized fluorophores on the side of the membrane is likely to be two dimensional. However, RET may display a different dimensionality for donors on the surface transferring to acceptors dispersed in the acyl side chain region. Also, acceptors on the opposite surface from the donor may contribute a three-dimensional component to the donor decay. While such systems can be interpreted in terms of fractal dimensions, the concept of fractal dimensions is rather abstract and does not always lead to physical insights. In these cases it is useful to consider a combination of energy transfer in two and three dimensions.

Energy transfer with a mixed dimensionality was found for the time-resolved donor decays from rhodamine 6G to malachite green, when both were bound to vesicles of dihexadecyl phosphate (DHP).[23] The donor decays are shown in Figure 15.9. In this case it was necessary to fit the data to a sum of eqs. 15.1 and 15.9. Although not shown, neither eqs. 15.1 or 15.9 alone provided a good fit to these data. While the authors interpreted this effect in terms of a non-random acceptor distribution, energy transfer across the bilayer could also have provided a component that appeared to be three dimensional. Once again, comparison of the steady-state data with predicted donor intensities was essential for selecting between distinct models.[23]

15.2.2. Experimental FRET in One Dimension

While there have been numerous studies of the time-resolved fluorescence of dyes bound to DNA,[31] there have been relatively few studies of RET for dyes intercalated into DNA.[32–35] In Figure 15.6 we showed simulations that indicated a rapidly decaying $t^{1/6}$ component for donors and acceptors in one dimension. Such time-dependent decays have been observed with dyes intercalated into poly d(A-T).[32] The donor was dimethyldiazaperopyrenium (DMPP) and the acceptor ethidium bromide (EB). Upon binding of the EB acceptor the DMPP emission was quenched, and the EB emission was enhanced (Figure 15.10). The time-domain data clearly show a fast component with increasing amplitude as the acceptor concentration is increased (Figure 15.11). Due to a lack of software the time-domain data were not analyzed in terms of eq. 15.12, but the shape of the decays is visually similar to the simulated data for RET in one dimension (Figure 15.6).

Useful information can also be obtained by examination of the steady-state data. For the D–A pair the observed transfer efficiency (Figure 15.10, insert) was found to be smaller than that predicted from Monte Carlo simulations. This result was explained as distortion of the DNA by binding of DMPP, which excluded EB from binding to nearby sites.

Energy transfer in one dimension was also studied using the frequency-domain method.[18] In this case the donor was acridine orange (AO) and the acceptor was the weakly fluorescent dye Nile blue (NB). Binding of NB at a low dye-per-base-pair ratio results in significant quenching of the AO emission (Figure 15.12). The FD intensity decay data are best fit by the equation for FRET in one dimension (Figure 15.13), indicating that energy transfer occurs in one dimension in this system.

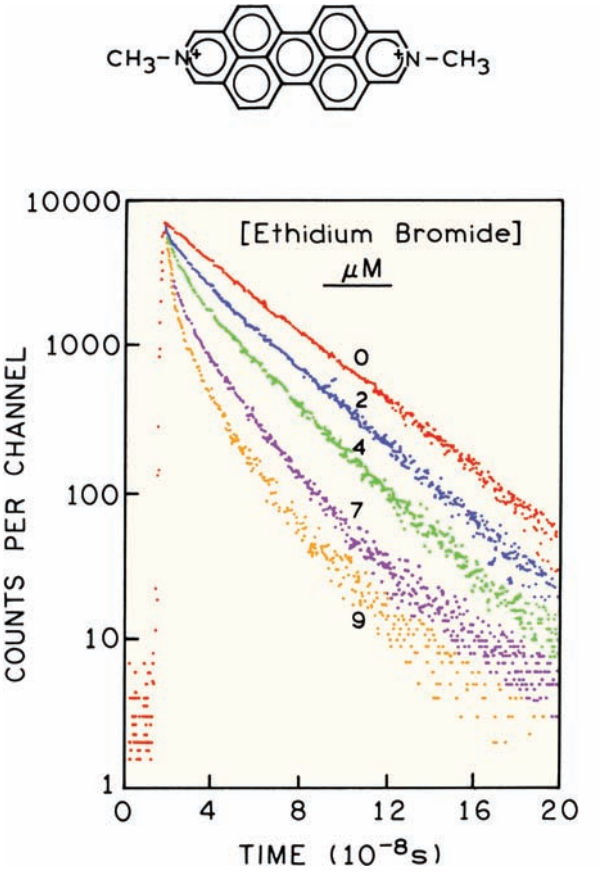

Figure 15.11. Intensity decay of dimethyldiazaperopyrenium bound to double stranded poly d (A-T) with increasing concentrations of ethidium bromide. Revised from [32].

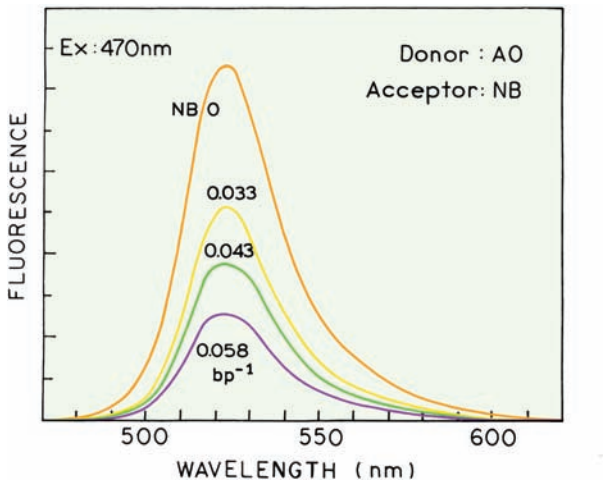

Figure 15.12. Emission spectra of acridine orange (AO) bound to DNA with increasing concentrations of Nile blue (NB) acceptor per DNA base pair. From [18]: Maliwal BP, Kusba J, Lakowicz JR. 1994. Fluorescence energy transfer in one dimension: frequency-domain fluorescence study of DNA-fluorophore complexes. *Biopolymers* 35:245–255. Copyright © 1994. Reprinted with permission from John Wiley and Sons Inc.

While the values of χ_R^2 support the 1D model, there are only minor visual differences between the fitted function for 1D, 2D, and 3D RET. However, analysis of the data should also include consideration of the parameter values and the reasonableness of these values. For eqs. 15.1, 15.9, and 15.12, once R_0 is known, the concentration is the only variable parameter. The concentrations recovered for NB from the analysis in Figure 15.13 are 0.058 acceptors/base pairs, 9.9 x 10^{11} molecules/cm^2, and 1.32 mM for the 1D, 2D, and 3D models, respectively. Based on one's understanding of the sample preparation it should be readily possible to exclude the 3D concentration of 1.32 mM. This is the concentration of acceptors in a 3D solution needed to result in energy transfer comparable to that observed for AO-DNA. The essential point is that one should always examine the desired parameters for reasonableness using one's chemical knowledge of the system. In our experience we found that the failure of parameter values to follow expected trends is often a sensitive indicator of the validity of the model, often more sensitive than the values of χ_R^2 themselves.

15.3. BIOCHEMICAL APPLICATIONS OF RET WITH MULTIPLE ACCEPTORS

15.3.1. Aggregation of β-Amyloid Peptides

The theory for RET with multiple acceptors is complex, but it is possible to use this type of RET without using the theory. It is known that deposition of the β-amyloid peptide in the brain is associated with Alzheimer's disease. This peptide contains about 40 amino acids and is known to undergo self-assembly or aggregation. This process was studied using a peptide sequence from the amyloid protein which contained the aggregation motif KLVFF near the center.

The complete sequence was EVHHQKLVFFAEDVG. This peptide was labeled with both a donor and acceptor. Figure 15.14 shows the donor lifetime distribution when the peptide is exposed to conditions that result in aggregation. Different lifetime distributions were obtained depending on the initial concentration of the peptide. The shortest overall lifetime was observed for an intermediate initial β-amyloid concentration. This result was interpreted as the effect of formation of a micelle-like aggregate at these concentrations, and an ordered β-sheet aggregate at higher concentra-

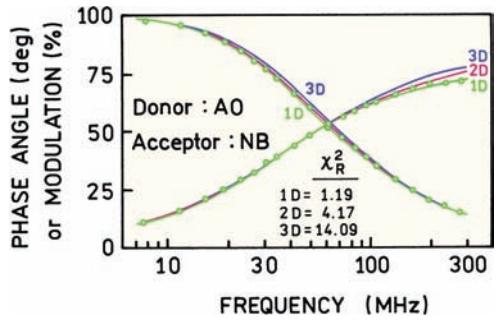

Figure 15.13. Frequency-domain intensity decay of AO-DNA with 0.058 NB/base pair. From [18]: Maliwal BP, Kusba J, Lakowicz JR. 1994. Fluorescence energy transfer in one dimension: frequency-domain fluorescence study of DNA-fluorophore complexes. *Biopolymers* 35:245–255. Copyright © 1994. Reprinted with permission from John Wiley and Sons Inc.

tions. In this example useful information was obtained from the RET data without using the theory needed to account for a distribution of multiple acceptors around the donors.

15.3.2. RET Imaging of Fibronectin

Fibronectin is a large protein that consists of globular regions connected by flexible linkers. Fibronectin (Fn) is secreted by cells such as fibroblasts and plays a role in assembly of extracellular matrix during development and

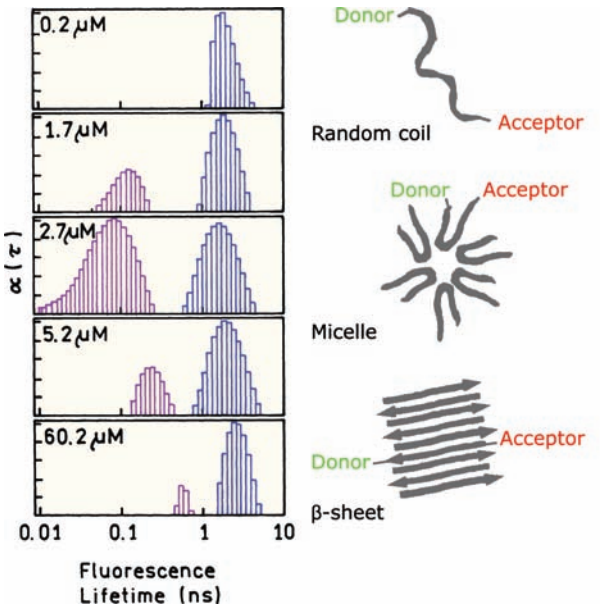

Figure 15.14. Lifetime distribution and aggregation schematic for β-amyloid. The donor was TMR and the acceptor was DABMI. Revised from [36].

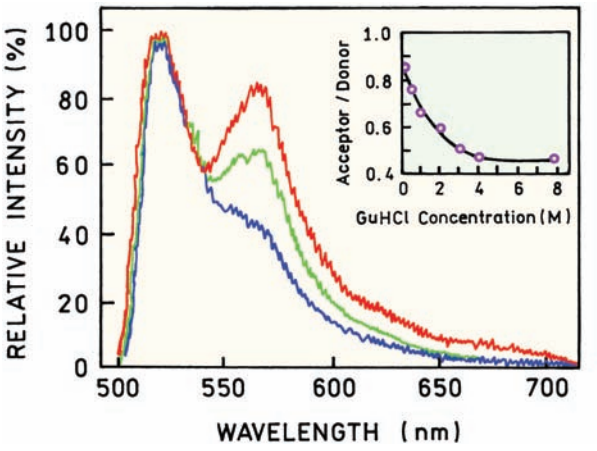

Figure 15.15. Emission spectra of fibronectin labeled with both Oregon green and TMR. From top to bottom at 570 nm the GuHCl concentrations are 0, 1.0, and 4.0 M. Revised from [37].

wound healing. Fn is thought to exist in a compact form that is not reactive with other extracellular matrix proteins, and in an extended form that interacts with collagen. RET was used to image the two forms of Fn without measuring D–A distances.

Fibronectin was labeled randomly with both Oregon green (OG) as the donor and TMR as the acceptor. In the compact form RET occurred between OG and TMR. Figure 15.15 shows emission spectra of the doubly labeled Fn. In the absence of GuHCl the Fn is in the compact state and there is obvious RET from TMR to OG. As the concentration of GuHCl is increased the acceptor emission decreases due to less efficient RET in the extended protein. The doubly labeled Fn was then incubated with 3T3 fibroblasts. In order to avoid RET between adjacent Fn molecules, labeled Fn was diluted tenfold with unlabeled Fn. The protein bound diffusely to the cell and to matrix fibrils (Figure 15.16). The cell was imaged with filters that transmitted the donor (green) or acceptor (orange) emission. These separate images were assigned colors and then overlaid. This image shows that the Fn that displays RET is diffusely bound to the cell. The Fn displaying stronger donor emission is found in the fibrils. This result shows that Fn can coexist in the compact or extended form depending upon its interaction with extracellular molecules.

15.4. ENERGY TRANSFER IN RESTRICTED GEOMETRIES

The theory described in Section 15.1 assumed a random distribution of acceptors, in one-, two-, or three-dimen-

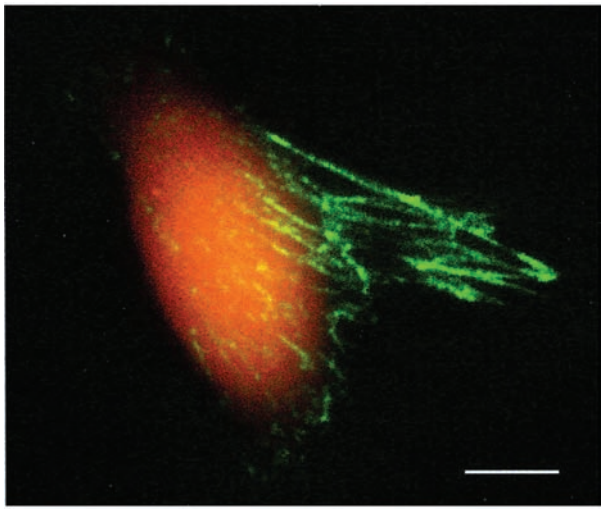

Figure 15.16. Psuedo-color image of fibronectin labeled with Oregon green and TMR on 3T3 fibroblasts. Scale bar is 10 μm. Revised from [37].

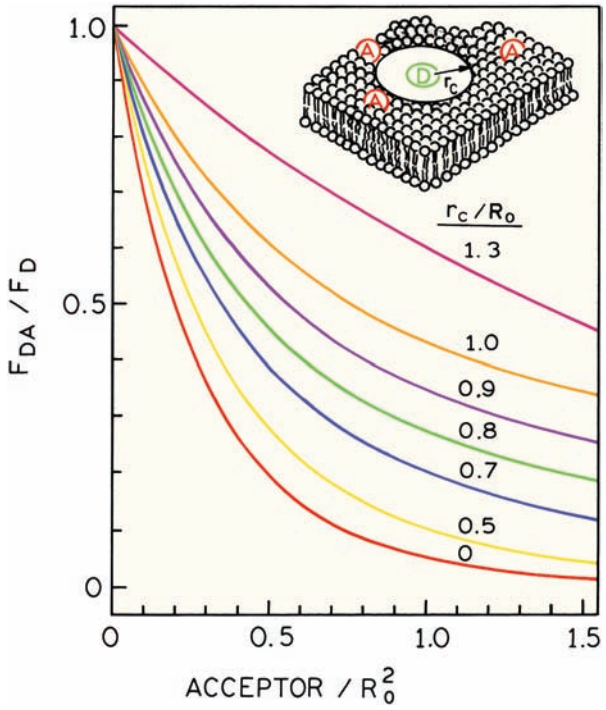

Figure 15.17. Relative donor yields for a random distribution of acceptors in two dimensions. r_C is the distance of closest approach of the donor and acceptor. Calculated according to [38] (see Table 15.2).

sions. One can imagine other situations when the acceptor distribution is non-random. For instance, consider a donor-labeled protein that is bound to a membrane. Depending on the size of the protein the acceptors may be excluded from a region directly around the donor. In this case the acceptor distribution would be random in two dimensions, but with a minimum distance between the donor and the nearest acceptor (Figure 15.17, insert). Many other non-random distributions can be imagined, such as DNA dyes with preferred binding to particular base sequences and distributions of charged acceptors around charged donors.

There have been several attempts to provide analytical expressions for a variety of geometric conditions. These attempts have resulted in complex expressions, which typically are valid under a limited range of conditions. For instance, an analytical solution for 2D RET was given, but this solution only applies when the distance of closest approach is (r_C) much less than R_0.[38] Another approximate solution was presented for the case where $r_C/R_0 > 0.7$.[39] Other solutions have been given,[40–48] but these complex formulas do not include D–A diffusion. Given the complexity of the equations and the range of possible conditions, there is merit in directly calculating the data for the desired geometry and D–A distribution. This can be accomplished by Monte Carlo[49] simulations or by use of numerical methods with general expressions.[50]

Monte Carlo simulations provide an ideal way to simulate the data for complex systems. The basic idea is to simulate data for one assumed configuration of the system, such as for a given number of acceptor molecules at given distances from the donor. This process is repeated many times, for random configurations generated for the assumed model. As stated by the authors, such simulations can be performed for systems of arbitrary complexity, and to any desired precision.[49] Another positive feature is that one does not need to derive an equation for the donor decay or donor intensity, but rather simply write the differential equation describing the donor. However, the necessary simulations can be time consuming even with modern computers, particularly if multiple Monte Carlo simulations must be done during the least-square fits.

Fortunately, there exists a general solution that can be used in systems of almost any complexity, in the absence of diffusion.[50] The basic idea is to use an integral equation to predict the intensity decay. In two dimensions these equations are

$$I_{DA}(t) = I_D^0 \exp(-t/\tau_D) \exp\left[-\sigma S(t)\right] \qquad (15.16)$$

where

$$S(t) = \int_{r_c}^{\infty} \{ 1 - \exp\left[-(t/\tau_D)(R_0/r)^6\right] \} \, 2\pi r \, dr \qquad (15.17)$$

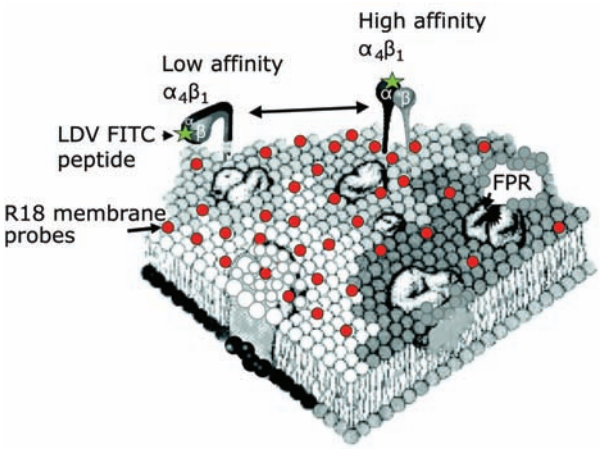

Figure 15.18. Schematic of a FITC-labeled peptide bound to the integrin αβ heterodimer in a plasma membrane. The red dots are the R18 acceptors. Reprinted with permission from [54].

The term $\exp[-\sigma S(t)]$ describes that portion of the donor decay due to energy transfer, σ is the surface density of the acceptor, and r_C is the distance of closest approach between the donors and acceptors. The expressions appropriate to one or three dimensions can be written by substituting the surface element $2\pi r$, with 2.0 or $4\pi r^2$, for a line or sphere, respectively. The donor intensity at time t can be calculated for any assumed probability distribution by numerical integration of the appropriate equation. The efficiency of transfer can be calculated from

$$E = 1 - \frac{\int_0^\infty I_{DA}(t)\,dt}{\int_0^\infty I_D(t)\,dt} \qquad (15.18)$$

While the use of these equations will be moderately complex, the approach is general and can be applied to most circumstances. For instance, the existence of an excluded volume around the donor is readily tested by changing the lower limits on the integral over distance. Example calculations using eqs. 15.16 and 15.17 were shown in Figures 13.28 and 13.31. The transfer efficiency was predicted using eqs. 15.16–15.18 as evidence for non-random distributions of donors and acceptors in membranes.[51–53] The basic idea is to compare the efficiency of energy transfer (eq. 15.18) with that calculated for a random distribution. Larger or smaller transfer efficiencies are taken to indicate co-localization or exclusion of the probes from areas containing the donor. It should be noted that the intensity decays of membrane-bound donors do not always agree with the model for RET in two dimensions.[53]

15.4.1. Effect of Excluded Area on Energy Transfer in Two Dimensions

Energy transfer from a donor to an acceptor in two dimensions is a frequently encountered model in membrane biophysics. Hence it is valuable to visualize how the donor intensities depend on the surface density of the acceptor and the distance of closest approach (r_C). These values can be obtained from approximation to the exact theory (Table 15.2).[38] The data in Table 15.2 provide a means to calculate the relative quantum yield of the donor using simple numerical equations. These data show that an excluded area results in a significant decrease in the transfer efficiency as soon as r_C exceeds $0.5R_0$. One can use the calculated values in Figure 15.17 for comparison with experimental data to estimate r_C.

Integrins are cell surface receptors that are present in all multicellular animals. Integrins provide adhesion of cells to each other and to extracellular matrices. Figure 15.18

Table 15.2. Numerical Parameters to Calculate the Relative Donor Quantum Yields in Membranes[a]

r_C/R_0	A_1	k_1	A_2	k_2
0.0	0.6463	4.7497	0.3537	2.0618
0.25	0.6290	4.5752	0.3710	1.9955
0.5	0.6162	4.0026	0.3838	1.4430
0.7	0.6322	3.1871	0.3678	0.7515
0.8	0.6344	2.7239	0.3656	0.4706
0.9	0.6336	2.2144	0.3664	0.2909
1.0	0.6414	1.7400	0.3586	0.1285
1.1	0.6327	1.3686	0.3673	0.04654[b]
1.3	0.6461	0.4899	0.3539	0.005633[b]

[a]From [38]. The relative quantum yields are given by $F_{DA}/F_D = A_1 \exp(-k_1C) + A_2 \exp(-k_2C)$, where C is the concentration of acceptor per R_0^2.

[b]These values seem to be incorrect in [38]. We decreased the published k_2 values by a factor of 10 and 100, for $r_C/R_0 = 1.1$ and 1.3, respectively. B. Hudson and P. Wolber confirmed that $k_2 = 0.04654$ at $r_C/R_0 = 1.1$.

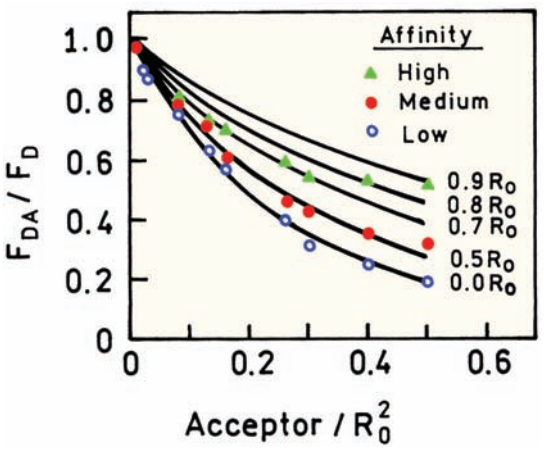

Figure 15.19. RET efficiency from the fluorescein label on integrin to membrane-bound R18. The lines are calculated from the theory in [38]. High affinity, 1 mM Mn^{2+}. Medium affinity, 1 mM Mn^{2+} and 1 mM Ca^{2+}. Low affinity, 1 mM Ca^{2+}. Revised from [54].

shows a schematic of the integrin αβ heterodimer bound to a plasma membrane. Integrin changes from a low-affinity state in the presence of Ca^{2+} to a high-affinity state in the presence of Mn^{2+}. It was thought that the low-affinity state was bent against the membrane and that the high-affinity state was extended away from the membrane. The approach shown in Figure 15.17 was used to study the conformation of membrane-bound integrin in each state.

Integrins are known to bind a short peptide (LDV) with high affinity. This peptide was labeled with FITC. The peptide bound to integrin and served as the donor. The acceptor was octadecylrhodamine (R18). The RET efficiency, as seen from the extent of donor quenching, was examined for a range of acceptor concentrations. The integrin was put into a high-, medium-, or low-affinity state by changing the concentrations of Ca^{2+} and Mn^{2+} (Figure 15.19). The extent of quenching was compared with that calculated for randomly distributed acceptors, but with an excluded area around the donor.[54] In the low-affinity state (○) the extent of donor quenching is consistent with the calculated values with no excluded area. In the high-affinity state the data are consistent with an excluded area with a radius r_C near $0.8R_0$, where R_0 is near 53 Å. The results suggested that the decrease in RET in the high-affinity state was due to both an excluded area and elevation of the donor above the membrane. These results show how the conformation of a membrane-bound protein can be studied using acceptors not directly linked to the protein.

15.5. RET IN THE PRESENCE OF DIFFUSION

In the previous examples we did not consider the effects of diffusion or the extent of energy transfer. For nanosecond-decay-time donors there is little effect on diffusion on energy transfer. However, if the donor lifetime exceeds about 100 ns then diffusion can result in increased transfer efficiency. One example is shown using simulated data in Figure 15.20. The figure shows simulated frequency-domain data for donors and acceptors randomly distributed in two dimensions.[55–57] These simulations were performed using a single acceptor concentration and a single lateral diffusion coefficient so that the changes are due to differences in the assumed donor lifetime. A diffusion coefficient of 5×10^{-8} cm^2/s was selected as typical for lipid diffusion in membranes. When the donor lifetime is 300 ns there is a small effect of diffusion indicated by the shaded area in Figure 15.20 (top panel). If the donor lifetime is 3 μs then diffusion can have a large effect, as seen from the shift in the frequency response to higher frequencies. These simulations show

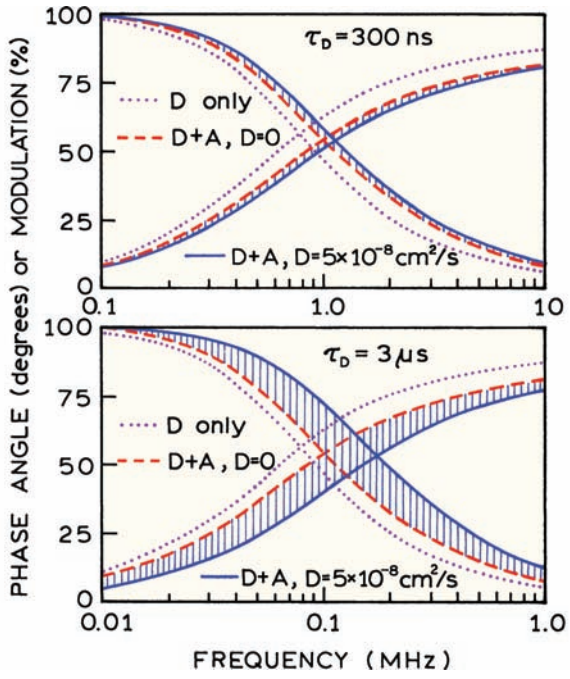

Figure 15.20. Simulated frequency-domain intensity decay for a donor and acceptor randomly distributed in two dimensions. For the simulations $R_0 = 25$ Å, $r_{min} = 7$ Å, 75 $Å^2$/lipid, 5×10^{-3} acceptors/lipid, and $D = 5 \times 10^{-8}$ cm^2 /s. The dashed lines show the expected donor decays without lateral diffusion, and the dotted lines show the donor decays in the absence of acceptors. Revised from [56].

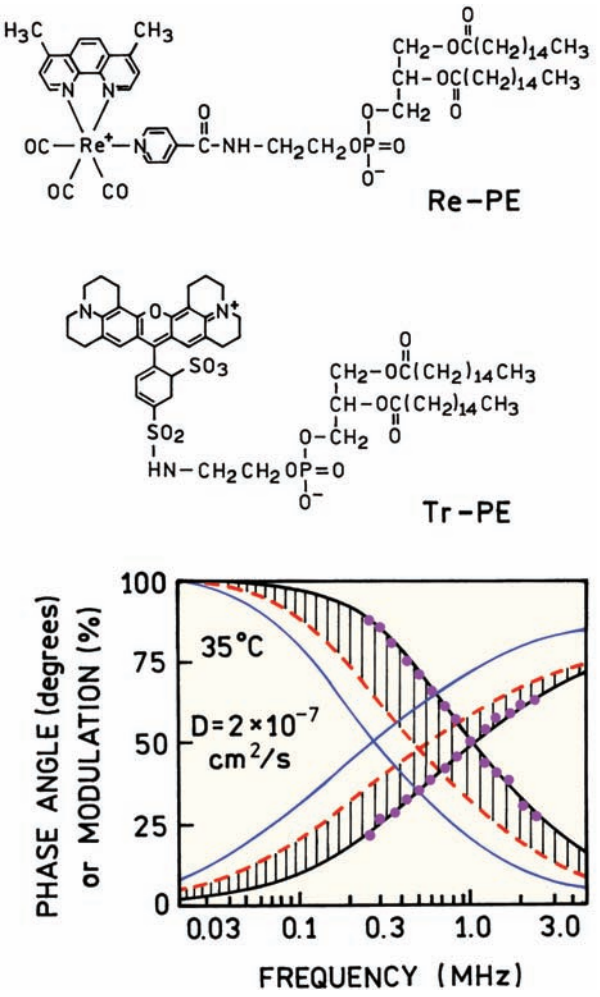

Figure 15.21. Re-PE donor decays in DOPC in the presence of a 0.02 mol fraction of Tr-PE acceptor. The solid line shows the best fit with the diffusion coefficient and acceptor density as variable parameters. The dashed line shows the predictive response at the known acceptor density and the diffusion coefficient set equal to zero. The thin solid line on the left is the donor in the absence of acceptor. Revised from [56].

that lipid diffusion in membranes will not affect the RET efficiency from ns-decay-time donors.

During the past 10 years a new class of probes has become available with decay times a fraction of a microsecond to several microseconds long (Chapter 20). These are transition metal–ligand complexes. One such rhenium complex synthesized as a lipid derivative is shown in Figure 15.21. The lifetime of this complex in the absence of acceptor can be longer than 2 μs, but is near 1 μs at 35°C in DOPC vesicles. The presence of 2 moles of acceptor decreases the mean decay time from 1.08 to 0.492 μs, with a recovered diffusion coefficient of 2 x 10^{-7} cm^2/s. If the diffusion coefficient is set to zero, with the acceptor concentration fixed at its known value, one obtains the dashed line. The shaded area represents the contribution of diffusion to decreasing the lifetime of the donor. The predicted donor decay is given by the dashed line. These results show that information on long-range diffusion can be obtained if long-decay-time donors are used.

15.6. RET IN THE RAPID DIFFUSION LIMIT

The theory for energy transfer in restricted geometries is complex, with or without diffusion. However, if the donor decay time is very long then the rapid diffusion limit is reached where the theory once again becomes relatively simple.[58–59]

The basic idea of energy transfer in the rapid diffusion limit is to use a donor lifetime (τ_D) and acceptor concentration such that the diffusion distance of the donor during τ_D is greater than the mean distance(s) between the donor and acceptor molecules. The rapid diffusion limit is reached when $D\tau_D/s^2 >> 1$, where $D = D_D + D_A$ is the mutual diffusion coefficient and s is the mean distance between D and A. There are several valuable consequences of being in the rapid diffusion limit.[58] The concentration of acceptors needed for RET can be 1000-fold less than in the static limit ($D\tau_D/s^2 << 1$), that is, μM rather than mM concentrations (Section 15.1). The donor intensity decays are single exponential because the acceptor distribution is averaged by diffusion, so that all donors see the same distribution. And, finally, the extent of transfer becomes limited by the distance of closest approach of the donor and acceptor, and can thus provide structural information about the investigated system.

What donor decay times are needed to reach the rapid diffusion limit? This question was addressed by numerical solution of the differential equations describing energy transfer in three dimensions.[7,58] Figure 15.22 shows the calculated transfer efficiencies for donors with various lifetimes when the acceptor concentration is 0.1 mM.[59] If the decay time is 1 ns there is little effect of diffusion on energy transfer, even for the highest possible diffusion coefficient of 10^{-5} cm^2/s in aqueous solution at room temperature. This is why D-to-A diffusion is often neglected in measurements of D–A distances, and why RET with ns-lifetime donors has not been used to measure domain dynamics in proteins.

If the donor lifetime is near 1 μs, the transfer efficiency becomes sensitive to diffusion. As shown above, such

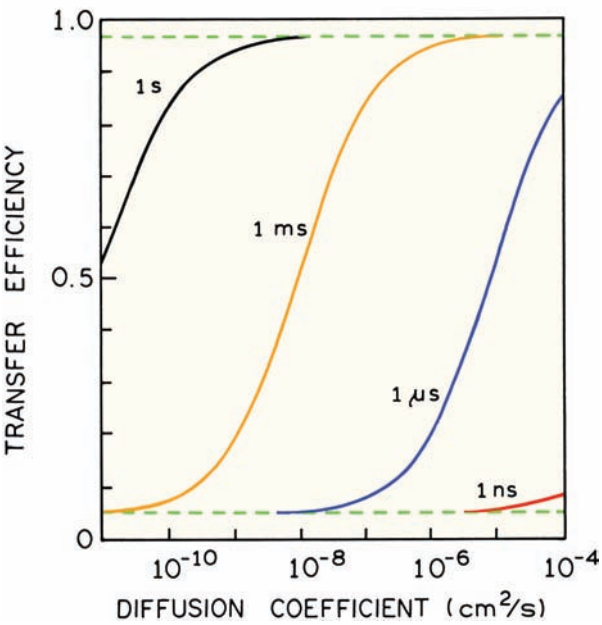

Figure 15.22. Calculated dependence of the transfer efficiency on the diffusion coefficient in three-dimensions for donor lifetimes τ_D of 1 ns, 1 μs, 1 ms, and 1 s. D is the sum of diffusion coefficients of the donor and acceptor. In this calculation, R_0 = 50 Å, r_C = 5 Å, and the acceptor concentration is 0.1 mM. Revised and reprinted with permission from [59]. Copyright © 1982, Annual Review Inc.

decay times are available using transition metal–ligand complexes. As the donor lifetime becomes longer, 1 ms to 1 s, the transfer efficiency reaches an upper limit. This is the rapid diffusion limit, which can be reached for diffusion coefficients exceeding 10^{-7} cm^2/s if the donor lifetimes are on the ms timescale. Such decay times are found in such lanthanides as europium or terbium, which display lifetimes near 2 ms.

Examination of Figure 15.22 reveals that the transfer efficiency reaches a limiting value less than 100% for high diffusion coefficients. This rapid diffusion limit is sensitive to the distance of closest approach of the donor to the acceptors. The transfer efficiency is given by

$$E = \frac{k_T}{\tau_D^{-1} + k_T} \tag{15.19}$$

where k_T is the sum of the transfer rates to all available acceptors. The transfer rate k_T can be calculated from the decay times measured in the absence (τ_D) and presence of acceptors (τ_{DA}):

$$k_T = \frac{1}{\tau_{DA}} - \frac{1}{\tau_D} \tag{15.20}$$

Because of diffusive averaging, it is relatively simple to calculate predicted values of k_T. The precise form of k_T depends on the geometric model, many of which have been described in detail.[58–62] For spherical donors and acceptors the diffusion-limited value of k_T is given by[58]

$$k_T = \rho_A \int_{r_c}^{\infty} \frac{1}{\tau_D} \left(\frac{R_0}{r}\right)^6 4\pi r^2 dr = \frac{4\pi\rho_A R_0^6}{3\tau_D r_C^3} \tag{15.21}$$

where ρ_A is the density of acceptors (molecules/Å^3) and r_C is the distance of closest approach. Equation 15.21 can be understood as the sum of all transfer rates to acceptors randomly distributed in three dimensions starting at r_C. The diffusion-limited transfer rate is thus dependent on r_C^{-3} and acceptor concentration. These values are shown in Figure 15.23 (top) for various acceptor concentrations. For r_C values less than 10 Å the transfer efficiencies can exceed 50% for an acceptor concentration of 10 μM, considerably lower than in the absence of diffusion (Section 15.1). This model can be used to measure the distance at which an acceptor is buried in a protein, using a long-lived donor. One such study measured transfer from terbium to the iron metal binding sites in protein transferrin.[61] From the transfer rates the iron sites were determined to be deeply buried in the protein, 17 Å below the surface.

Suppose one had a long-lived lipid derivative that served as the donor within a membrane also containing acceptors. In two dimensions the diffusion-limited rate constant is given by

$$k_T = \frac{1}{\tau_D} \int_{r_c}^{\infty} \left(\frac{R_0}{r}\right)^6 \sigma_A 2\pi r\, dr = \frac{\pi\sigma_A R_0^6}{\tau_D 2r_C^4} \tag{15.22}$$

where σ_A is in acceptors/Å^2. Hence in two dimensions the transfer efficiency is proportional to r_C^{-4}, whereas in three dimensions it is proportional to r_C^{-3}. Given the simplicity of calculating k_T, these expressions have been obtained for a variety of geometric models.[59]

15.6.1. Location of An Acceptor in Lipid Vesicles

Diffusion-limited energy transfer has also been applied to membrane-bound fluorophores, but to a case different from

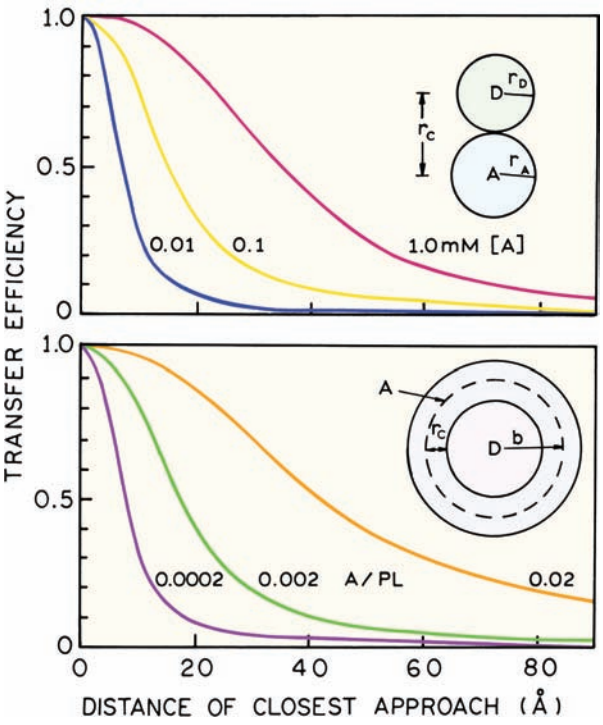

Figure 15.23. Effect of the distance of closest approach (r_C) between the donor and acceptor on the transfer efficiency in the rapid-diffusion limit. $R_0 = 50$ Å in this calculation. Top: Solution of donors and acceptors. The acceptor concentrations are 1.0, 0.1, and 0.01 mM. Bottom: Solution of donors trapped in the inner aqueous space of a membrane vesicle containing a spherical shell of acceptors at radius $b = 150$ Å. The surface densities of acceptor are 0.02, 0.002, and 0.0002 per phospholipid (acceptors per 70 Å^2). Revised from [58].

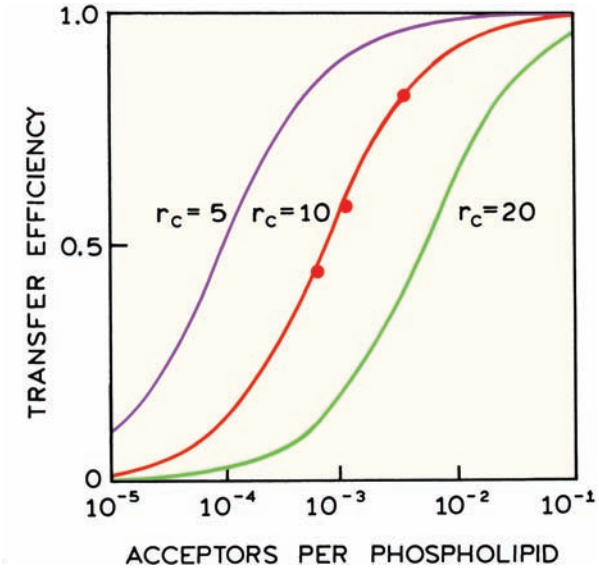

Figure 15.24. Diffusion-limited energy transfer from $Tb(DPA)_3$ trapped in the inner volume of egg PC vesicles labeled with eosin-phosphatidylethanolamine as the acceptor. The solid lines were calculated using eq. 15.23 assuming $R_0 = 45.6$ Å and $b = 150$ Å, and assuming an area of 70 Å^2 per phospholipid. Revised from [58].

lateral diffusion (eq. 15.22). One example shown in Figure 15.23 (bottom) is for donors trapped in the internal aqueous region of a vesicle of radius b. The acceptors are at a known surface density (σ_A in molecules/Å^2) located at a distance r_C below the surface. The diffusion-limited transfer rate is given by

$$k_T = \frac{3\pi b \sigma_A R_0^6}{2\tau_D (b - r_C)^3} \left[\frac{1}{2} \{ (2b - r_C)^{-2} - r_C^{-2} \} \right.$$

$$\left. + \frac{b}{3} \{ r_C^{-3} - (2b - r_C)^{-3} \} \right] \qquad (15.23)$$

These values are shown in Figure 15.23 (bottom) for various surface densities of the acceptor. Energy transfer can be 50% efficient for only 1 acceptor per 5000 phospholipids, if the distance of closest approach is 10 Å.

This model was applied to egg phosphatidylcholine vesicles labeled with eosin-phosphatidylethanolamine (eosin-PE) as the acceptor. The donor was $Tb(DPA)_3$, where DPA is dipicolinic acid. The donor was trapped in the internal aqueous volume of the vesicles. Energy transfer from the $Tb(DPA)_3$ to the eosin acceptor was about 50% efficient at just one acceptor per 1000 phospholipid molecules (Figure 15.24). The distance of closest approach of $Tb(DPA)_3$ to eosin was determined by comparison with curves calculated using eq. 15.23. The overall diameter of the vesicles was estimated by electron microscopy, allowing b to be fixed at 150 Å. The extent of energy transfer was consistent with a distance of closest approach of 10 Å (Figure 15.24), suggesting the eosin was localized just under the surface of the membrane. It was not necessary to consider eosin in the outer bilayer since the distance of closest approach determined the transfer efficiency.

15.6.2. Location of Retinal in Rhodopsin: Disc Membranes

The model of a long-lived donor trapped in vesicles was applied to rhodopsin, the photoreceptor protein in retinal rods. This membrane-bound protein contains a retinal chromophore, which serves as the acceptor (Figure 15.25).[60,63] It

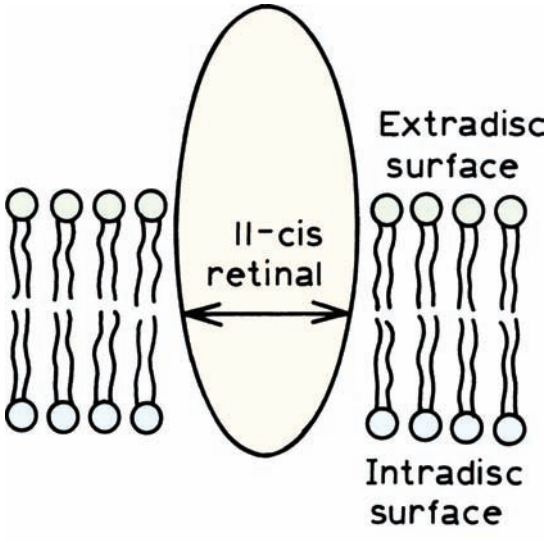

Figure 15.25. Schematic diagram of rhodopsin in a membrane. The single retinal moiety is placed midway between the membrane surfaces, roughly consistent with the energy transfer data. Reprinted with permission from [60]. Copyright © 1982, Academic Press Inc.

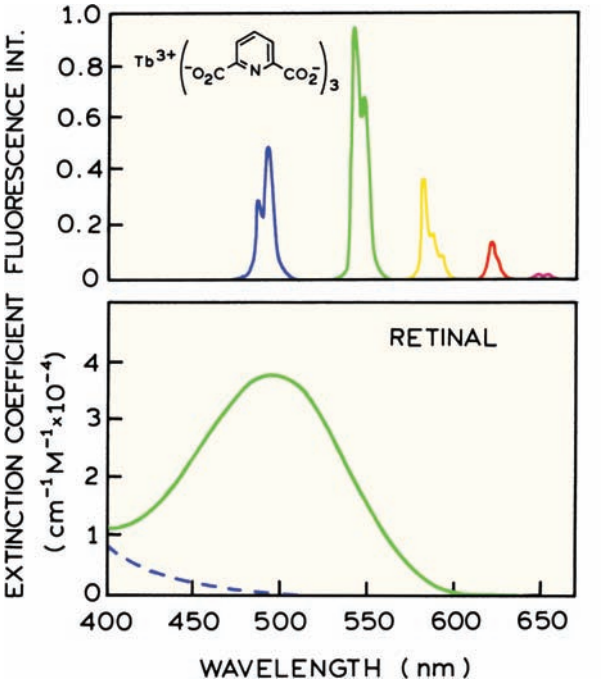

Figure 15.26. **Top**: Emission spectrum of the donor terbium dipicolinate. **Bottom**: Absorption spectrum of the retinal acceptor, before (solid) and after (dashed) photobleaching. Reprinted with permission from [60]. Copyright © 1982, Academic Press Inc.

was possible to prepare vesicles containing rhodopsin that had the same sidedness as native disc membranes.

The absorption spectrum of the acceptor is shown in Figure 15.26. Fortunately, retinal can be photobleached, thus decreasing the acceptor concentration in the disc membranes. Prior to photobleaching its absorption spectrum overlaps with that of the Tb^{3+} donor. The emission spectrum of terbium is typical of the lanthanides. The emission is from *f* orbitals of the atom, and typically consist of highly structured line spectra. Also, it is common to use lanthanide chelates, rather than lanthanides alone. This is because the lanthanides are extremely weak absorbers, with extinction coefficients near 0.1 M^{-1} cm^{-1}. Fortunately, lanthanides can be chelated with aromatic absorbers such as dipicolinate (Figure 15.26). Light absorbed by the ligand is efficiently transferred to the Tb^{3+}, resulting in effective absorption coefficients orders of magnitude larger than the uncomplexed lanthanides.

In order to localize the retinal in membranes, terbium was added to the inside or outside of vesicles. Intensity decays for Tb^{3+} trapped inside the disc vesicles are shown in Figure 15.27. The intensity decay is a single exponential in the absence and presence of rhodopsin as predicted for diffusive averaging. The Tb^{3+} decays as a single exponential in the presence of acceptors because all of the Tb^{3+} donor

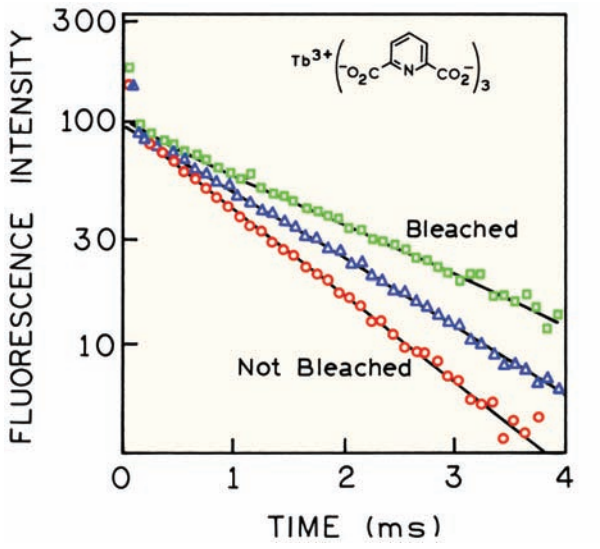

Figure 15.27. Emission kinetics of terbium dipicolinate trapped inside disc membrane vesicles. The fluorescence intensity (plotted on a logarithmic scale) is shown as a function of time after a 1-μs exciting light pulse. Circles (fastest decay), unbleached membranes; triangles, partially bleached; squares, completely bleached. Revised from [60].

experience the same diffusion-limited rate of transfer. Photobleaching of the retinal decreases its effective concentration, and the Tb^{3+} lifetime increases.

The decay times found for Tb^{3+} within the vesicles can be used to determine the transfer efficiency. Since the intensity decays are single exponentials, the efficiency can be calculated from

$$E = 1 - \frac{\tau_{DA}}{\tau_D} \tag{15.24}$$

where τ_{DA} and τ_D are the Tb^{3+} decay times in the presence and in the absence of energy transfer. The transfer efficiency is then compared with that predicted using eq. 15.23 to determine the retinal distance below the inner membrane surface. The distance of retinal from the inner membrane surface was estimated to be 22 Å.

15.7. CONCLUSIONS

The phenomenon of Förster transfer is simultaneously simple and complex. While the theory describing the mechanism of dipolar transfer is complex, the result is dependable and robust. Förster distances can be predicted with good accuracy from the spectral properties of the donor and acceptor. There are no known exceptions to Förster transfer, so that RET can be reliably assumed to occur whenever the donors and acceptors are in close proximity. Hence, RET is a reliable method to study the proximity and geometric distributions of donor–acceptor pairs.

The complexity of energy transfer arises from the occurrence of distance distributions, non-random distributions, and donor-to-acceptor diffusion. These phenomena result in complex theory, not because of Förster transfer, but because of the need to average the distance dependence over various geometrics and timescales.

REFERENCES

1. Förster Th. 1949. Experimentelle und theoretische Untersuchung des zwischenmolekularen Ubergangs von Elektronenanregungsenergie. *Z Naturforsch A* **4**:321–327.
2. Förster Th. 1959. 10th Spiers memorial lecture, transfer mechanisms of electronic excitation. *Discuss Faraday Soc* **27**:7–17.
3. Bojarski C, Sienicki K. 1990. Energy transfer and migration in fluorescent solutions. In *Photochemistry and photophysics*, Vol. I, pp. 1–57. Ed JF Rabek. CRC Press, Boca Raton, GL.
4. Galanin MD. 1955. The influence of concentration on luminescence in solutions. *Sov Phys JETP* **1**:317–325.
5. Maksimov MA, Rozman IM. 1962. On the energy transfer in rigid solutions. *Opt Spectrosc* **12**:337–338.
6. Elkana Y, Feitelson J, Katchalski E. 1968. Effect of diffusion on transfer of electronic excitation energy. *J Chem Phys* **48**:2399–2404.
7. Steinberg IZ, Katchalski E. 1968. Theoretical analysis of the role of diffusion in chemical reactions, fluorescence quenching, and nonradiative energy transfer. *J Chem Phys* **48**(6):2404–2410.
8. Kusba J. 1987. Long-range energy transfer in the case of material diffusion. *J Luminesc* **37**:287–291.
9. Yokota M, Tanimato O. 1967. Effects of diffusion on energy transfer by resonance. *J Phys Soc Jpn* **22**(3):779–784.
10. Gösele U, Hauser M, Klein UKA, Frey R. 1975. Diffusion and long-range energy transfer. *Chem Phys Lett* **34**(3):519–522.
11. Faulkner LR. 1976. Effects of diffusion on resonance energy transfer: comparisons of theory and experiment. *Chem Phys Lett* **43**(6): 552–556.
12. Millar DP, Robbins RJ, Zewail AH. 1981. Picosecond dynamics of electronic energy transfer in condensed phases. *J Chem Phys* **75**(8): 3649–3659.
13. Lakowicz JR, Szmacinski H, Gryczynski I, Wiczk W, Johnson ML. 1990. Influence of diffusion on excitation energy transfer in solutions by gigahertz harmonic content frequency-domain fluorometry. *J Phys Chem* **94**:8413–8416.
14. Birks JB, Georghiou S. 1968. Energy transfer in organic systems, VII: effect of diffusion on fluorescence decay. *J Phys B* **1**:958–965.
15. Tweet AO, Bellamy WD, Gains GL. 1964. Fluorescence quenching and energy transfer in monomolecular films containing chlorophyll. *J Chem Phys* **41**:2068–2077.
16. Koppel DE, Fleming PJ, Strittmatter P. 1979. Intramembrane positions of membrane-bound chromophores determined by excitation energy transfer. *Biochemistry* **24**:5450–5457.
17. Szmacinski H. 1998. Personal communication.
18. Maliwal BP, Kusba J, Lakowicz JR. 1994. Fluorescence energy transfer in one dimension: frequency-domain fluorescence study of DNA–fluorophore complexes. *Biopolymers* **35**:245–255.
19. Drake JM, Klafter J, Levitz P. 1991. Chemical and biological microstructures as probed by dynamic processes. *Science* **251**:1574–1579.
20. Dewey TG. 1991. Excitation energy transport in fractal aggregates. *Chem Phys* **150**:445–451.
21. Lianos P, Duportail G. 1993. Time-resolved fluorescence fractal analysis in lipid aggregates. *Biophys Chem* **48**:293–299.
22. Loura LMM, Fedorov A, Prieto M. 1996. Resonance energy transfer in a model system of membranes: applications to gel and liquid crystalline phases. *Biophys J* **71**:1823–1836.
23. Tamai N, Yamazaki T, Yamazaki I, Mizuma A, Mataga N. 1987. Excitation energy transfer between dye molecules adsorbed on a vesicle surface. *J Phys Chem* **91**:3503–3508.
24. Levitz P, Drake JM, Klafter J. 1988. Critical evaluation of the application of direct energy transfer in probing the morphology of porous solids. *J Chem Phys* **89**(8):5224–5236.
25. Drake JM, Levitz P, Sinha SK, Klafter J. 1988. Relaxation of excitations in porous silica gels. *Chem Phys* **128**:199–207.
26. Dewey TG, Datta MM. 1989. Determination of the fractal dimension of membrane protein aggregates using fluorescence energy transfer. *Biophys J* **56**:415–420.

27. Drake JM, Kafter J. 1990. Dynamics of confined molecular systems. *Phys Today*, May, pp. 46–55.
28. Pines D, Huppert D. 1987. Time-resolved fluorescence depolarization measurements in mesoporous silicas: the fractal approach. *J Phys Chem* **91**(27):6569–6572.
29. Pines D, Huppert D, Avnir D. 1988. The fractal nature of the surfaces of porous silicas as revealed in electronic energy transfer between adsorbates: comparison of three donor/acceptor pairs. *J Chem Phys* **89**:1177–1180.
30. Nakashima K, Duhamel J, Winnik MA. 1993. Photophysical processes on a latex surface: electronic energy transfer from rhodamine dyes to malachite green. *J Phys Chem* **97**:10702–10707.
31. Schurr JM, Fujimoto BS, Wu P, Song L. 1992. Fluorescence studies of nucleic acids: dynamics, rigidities and structures. In *Topics in fluorescence spectroscopy*, Vol. 3: *Biochemical applications*, pp. 137–229. Ed JR Lakowicz. Plenum Press, New York.
32. Mergny J-L, Slama-Schwok A, Montenay-Garestier T, Rougee M, Helene C. 1991. Fluorescence energy transfer between dimethyldiazaperopyrenium dication and ethidium intercalated in poly d(A-T). *Photochem Photobiol* **53**(4):555–558.
33. Lee BW, Moon SJ, Youn MR, Kim JH, Jang HG, Kim SK. 2003. DNA mediated resonance energy transfer from 4',6-diamidino-2-phenylindole to $[Ru(1,10\text{-phenanthroline})_2L]^{2+}$. *Biophys J* **85**:3865–3871.
34. Murata S, Kusba J, Piszczek G, Gryczynski I, Lakowicz JR. 2000. Donor fluorescence decay analysis for energy transfer in double-helical DNA with various acceptor concentrations. *Biopolymers* **57**: 306–315.
35. Kang JS, Lakowicz JR, Piszczek G. 2002. DNA dynamics: a fluorescence resonance energy transfer study using a long-lifetime metal–ligand complex. *Arch Pharm Res* **25**(2):143–150.
36. Kim J, Lee M. 2004. Observation of multi-step conformation switching in β-amyloid peptide aggregation by fluorescence resonance energy transfer. *Biochem Biophys Res Commun*. **316**:393–397.
37. Baneyx G, Baugh L, Vogel V. 2001. Coexisting conformations of fibronectin in cell culture imaged using fluorescence resonance energy transfer. *Proc Natl Acad Sci USA* **98**(25):14454–14468.
38. Wolber PK, Hudson BS. 1979. An analytic solution to the Förster energy transfer problem in two dimensions. *Biophys J* **28**:197–210.
39. Dewey TG, Hammes GG. 1986. Calculation of fluorescence resonance energy transfer on surfaces. *Biophys J* **32**:1023–1036.
40. Hauser M, Klein UKA, Gosele U. 1976. Extension of Förster's theory for long-range energy transfer to donor–acceptor pairs in systems of molecular dimensions. *Z Phys Chem* **101**:255–266.
41. Estep TN, Thompson TE. 1979. Energy transfer in lipid bilayers. *Biophys J* **26**:195–208.
42. Dobretsov GE, Kurek NK, Machov VN, Syrejshchikova TI, Yakimenko MN. 1989. Determination of fluorescent probes localization in membranes by nonradiative energy transfer. *J Biochem Biophys Methods* **19**:259–274.
43. Blumen A, Klafter J, Zumofen G. 1986. Influence of restricted geometries on the direct energy transfer. *J Chem Phys* **84**(3):1307–1401.
44. Kellerer H, Blumen A. 1984. Anisotropic excitation transfer to acceptors randomly distributed on surfaces. *Biophys J* **46**:1–8.
45. Yguerabide Y. 1994. Theory of establishing proximity relationships in biological membranes by excitation energy transfer measurements. *Biophys J* **66**:683–693.
46. Bastiaens P, de Beun A, Lackea M, Somerharja P, Vauhkomer M, Eisinger J. 1990. Resonance energy transfer from a cylindrical distribution of donors to a plan of acceptors: location of apo-B100 protein on the human low-density lipoprotein particle. *Biophys J* **58**:665–675.
47. Baumann J, Fayer MD. 1986. Excitation transfer in disordered two-dimensional and anisotropic three-dimensional systems: effects of spatial geometry on time-resolved observables. *J Chem Phys* **85**: 4087–4107.
48. Zimet DB, Thevenin BJ-M, Verkman AS, Shohet SB, Abney JR. 1995. Calculation of resonance energy transfer in crowded biological membranes. *Biophys J* **68**:1592–1603.
49. Snyder B, Frieri E. 1982. Fluorescence energy transfer in two dimensions. *Biophys J* **40**:137–148.
50. Fung B, Stryer L. 1978. Surface density measurements in membranes by fluorescence resonance energy transfer. *Biochemistry* **17**: 5241–5248.
51. Pedersen S, Jorgensen K, Baekmark TR, Mouritsen OG. 1996. Indirect evidence for lipid-domain formation in the transition region of phospholipid bilayers by two-probe fluorescence energy transfer. *Biophys J* **71**:554–560.
52. Wolf DE, Winiski AP, Ting AE, Bocian KM, Pagano RE. 1992. Determination of the transbilayer distribution of fluorescent lipid analogues by nonradiative fluorescence resonance energy transfer. *Biochemistry* **31**:2865–2873.
53. Shaklai N, Yguerabide J, Ranney HM. 1977. Interaction of hemoglobin with red blood cell membranes as shown by a fluorescent chromophore. *Biochemistry* **16**(25):5585–5592.
54. Chigaev Z, Buranda T, Dwyer DC, Prossnitz ER, Sklar LA. 2003. FRET detection of cellular α_4-integrin conformational activation. *Biophys J* **85**:3951–3962.
55. Kusba J, Piszczek G, Gryczynski I, Johnson ML, Lakowicz JR. 2000. Effects of diffusion on energy transfer in solution using a microsecond decay time rhenium metal–ligand complex as the donor. *Chem Phys Letts* **319**:661–668.
56. Kusba J, Li L, Gryczynski I, Piszczek G, Johnson ML, Lakowicz JR. 2002. Lateral diffusion coefficients in membranes measured by resonance energy transfer and a new algorithm for diffusion in two dimensions. *Biophys J* **82**:1358–1372.
57. Kusba J, Lakowicz JR. 1994. Diffusion-modulated energy transfer and quenching: analysis by numerical integration of diffusion equation in laplace space. *Methods Enzymol* **240**:216–262.
58. Thomas DD, Carlsen WF, Stryer L. 1978. Fluorescence energy transfer in the rapid diffusion limit. *Proc Natl Acad Sci USA* **75**:5746–5750.
59. Stryer L, Thomas DD, Meares CF. 1982. Diffusion-enhanced fluorescence energy transfer. *Annu Rev Biophys Bioeng* **11**:203–222.
60. Thomas DD, Stryer L. 1982. Transverse location of the retinal chromophore of rhodopsin in rod outer segment disc membranes. *J Mol Biol* **154**:145–157.
61. Yeh SM, Meares CF. 1980. Characterization of transferrin metal-binding sites by diffusion-enhanced energy transfer. *Biochemistry* **19**:5057–5062.

62. Wensel TG, Chang C-H, Meares CF. 1985. Diffusion-enhanced lanthanide energy-transfer study of DNA-bound cobalt(III) bleomycins: comparisons of accessibility and electrostatic potential with DNA complexes of ethidium and acridine orange. *Biochemistry* **24**: 3060–3069.
63. Stryer L, Thomas DD, Carlsen WF. 1982. Fluorescence energy transfer measurements of distances in rhodopsin and the purple membrane protein. *Methods Enzymol* **81**:668–678.
64. Duportail G, Merola F, Lianos P. 1995. Fluorescence energy transfer in lipid vesicles: a time-resolved analysis using stretched exponentials. *J Photochem Photobiol A Chem* **89**:135–140.

ADDITIONAL REFERENCES ON RET BETWEEN UNLINKED DONOR AND ACCEPTOR

Experimental

Gupta RR, Ramachandra Rao VS, Watkins JJ. 2003. Measurement of probe diffusion in CO_2-swollen polystyrene using in situ fluorescence nonradiative energy transfer. *Macromolecules* **36**:1295–1303.

Martin IR, Rodriguez VD, Rodriguez-Mendoza UR, Lavin V. 1999. Energy transfer with migration: generalization of the Yokota-Tanimoto model for any kind of multipole interaction. *J Chem Phys* **111**(3):1191–1194.

Membranes

Barrantes FJ. 2001. Fluorescence studies of the acetylcholine receptor: structure and dynamics in membranes and cells. *J Fluoresc* **11**(4): 273–285.

Gorbenko GP, Domanov YA. 2002. Energy transfer method in membrane studies: some theoretical and practical aspects. *J Biochem Biophys Methods* **52**:45–58.

Jones GM, Wofsy C, Aurell C, Sklar LA. 1999. Analysis of vertical fluorescence resonance energy transfer from the surface of a small-diameter sphere. *Biophys J* **76**:517–527.

Loura LMS, Castanho MARB, Fedorov A, Prieto M. 2001. A photophysical study of the polyene antibiotic filipin self-aggregation and filipin-ergosterol interaction. *Biochim Biophys Acta* **1510**:125–135.

Loura LMS, Castanho MARB, Fedorov A, Prieto M. 2001. Fluid–fluid membrane microheterogeneity: a fluorescence resonance energy transfer study. *Biophys J* **80**:776–788.

Loura LMS, de Almeida RFM, Prieto M. 2001. Detection and characterization of membrane microheterogeneity by resonance energy transfer. *J Fluoresc* **11**(3):197–209.

Matko J, Edidin M. 1997. Energy transfer methods for detecting molecular clusters on cell surfaces. *Methods Enzymol* **278**:444–462.

Silvius JR, 2003. Fluorescence energy transfer reveals microdomain formation at physiological temperatures in lipid mixtures modeling the outer leaflet of the plasma membrane. *Biophys J* **85**:1034–1045.

Micelles

De S, Girigoswami A. 2004. Fluorescence resonance energy transfer—a spectroscopic probe for organized surfactant media. *J Colloid Interface Sci* **271**:485–495.

Particles

Arnold S, Holler S, Druger SD. 1996. Imaging enhanced energy transfer in a levitated aerosol particle. *J Chem Phys* **104**(19):7741–7748.

Arnold S, 1997. Cavity-enhanced fluorescence decay rates from microdroplets. *J Chem Phys* **106**(19):8280–8282.

Barnes MD, Whitten WB, Ramsey JM. 1994. Probing femtosecond dynamics in solution on a picosecond time scale: cavity enhancement of spontaneous emission rates in microdroplets. *Chem Phys Lett* **227**: 628–632.

Caruso F, Donath E, Möhwald H. 1998. Influence of polyelectrolyte multilayer coatings on Förster resonance energy transfer between 6-carboxyfluorescein and rhodamine B-labeled particles in aqueous solution. *J Phys Chem B* **102**:2011–2016.

Druger SD, Arnold S, Folan LM. 1987. Theory of enhanced energy transfer between molecules embedded spherical dielectric particles. *J Chem Phys* **87**:2649–2659.

Gan D, Lyon LA. 2001. Interfacial nonradiative energy transfer in responsive core-shell hydrogel nanoparticles. *J Am Chem Soc* **123**:8203–8209.

Jeuris K, Vanoppen P, De Schryver FC, Hofstraat JW, van der Ven LGJ, van Velde JW. 1998. Fluorescence intensity of dye containing latex particles studied by near-field scanning optical microscopy. *Macromolecules* **31**:8579–8584.

Li. Y, Kuwabara H, Gong Y-K, Takaki Y, Nakashima K. 2003. Resonance energy transfer from dibucaine to acriflavine in polystyrene latex dispersions. *J Photochem Photobiol B: Biol* **70**:171–176.

Polymers

Tcherkasskaya O, Spiro JG, Ni S, Winnik MA. 1996. Energy transfer in restricted geometry: polyisoprene-poly(methyl methacrylate) block copolymer interfaces. *J Phys Chem* **100**:7114–7121.

Tcherkasskaya O, Ni S, Winnik MA. 1996. Direct energy transfer studies of the domain-boundary interface in polyisoprene–poly(methyl methacrylate) block copolymer films. *Macromolecules* **29**:610–616.

Tcherkasskaya O, Ni S, Winnik MA. 1997. Energy transfer studies of binary block copolymer blends, 1: effect of composition on the interface area per chain and the lamellar size. *Macromolecules* **30**:2623–2632.

Yekta A, Spiro JG, Winnik MA. 1998. A critical evaluation of direct energy transfer as a tool for analysis of nanoscale morphologies in polymers: application to block copolymer interfaces. *J Phys Chem B* **102**:7960–7970.

Theory, Assemblies

de Jonge JJ, Ratner MA, de Leeuw SW, Simonis RO. 2004. Molecular dipole chains, III: energy Transfer. *J Phys Chem B* **108**:2666–2675.

Scholes GD, Jordanides XJ, Fleming GR. 2001. Adapting the Förster theory of energy transfer for modeling dynamics in aggregated molecular assemblies. *J Phys Chem B* **105**:1640–1651.

Theory without Diffusion

Rolinski OJ, Birch DJS. 2000. Determination of acceptor distribution from fluorescence resonance energy transfer: theory and simulation. *J Chem Phys* **112**(20):8923–8933.

Yekta A, Winnik MA, Farinha JPS, Martinho JMG. 1997. Dipole–dipole electronic energy transfer: fluorescence decay functions for arbitrary distributions of donors and acceptors, II: systems with spherical symmetry. *J Phys Chem A* **101**:1787–1792.

Theory With Diffusion

Bandyopadhyay T, Ghosh SK. 2003. Diffusion-assisted end-to-end relaxation of a flexible Rouse polymer chain: fluorescence quenching through a model energy transfer. *J Chem Phys* **119**(1):572–584.

Güzntürk KS, Giz AT, Pekcan Ö. 1998. Monte-Carlo simulation of fluorescence decay profiles during interdiffusion of donor–acceptor spheres to mimic latex film formation. *Eur Polym J* **34**(5/6):789–795.

Krishna MMG, Das R, Periasamy N, Nityananda R. 2000. Translational diffusion of fluorescent probes on a sphere: Monte Carlo simulations, theory, and fluorescence anisotropy experiments. *Chem Phys* **112**(19):8502–8514.

PROBLEMS

P15.1. *Estimation of the Distance of Closest Approach (r_C) for Donor and Acceptor Lipids in Vesicles*: Egg yolk phosphatidylethanolamine (PE) vesicles were prepared containing donors and acceptors. The donor was N-(7-nitrobenz-2-oxa-1,3-diazol-4-yl)-phosphatidylethanolamine (NBD-PE). The acceptor was N-(lissamine-rhodamine-â-sulfonyl)-phosphatidyl ethanolamine (Rh-PE).[64] Emission spectra are shown in Figure 15.28.

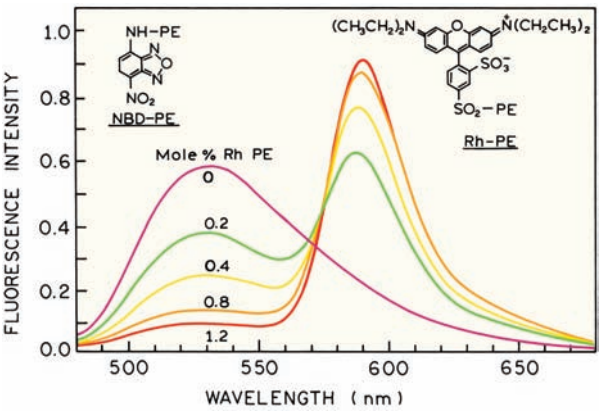

Figure 15.28. Emission spectra of egg yolk phosphatidylethanolamine vesicles containing 1 mole% NBD-PE and the indicated mole% of Rh-PE. Excitation wavelength 455 nm. Revised from [64].

Estimate the distance of closest approach of NBD-PE and Rh-PE. Assume a phospholipid molecule (PE) occupies 70 Å^2 and that the Förster distance is 50 Å. How could the measured donor quenching exceed the maximum predicted quenching in Figure 15.17?

P15.2. *Calculation of the Maximum Transfer Rate for Diffusion-Limited Quenching*: Wensel et al.[62] examined quenching of a positively charged terbium chelate by ethidium bromide bound to double-helical DNA. In the presence of DNA alone the decay time was 0.844 ms, and in the presence of DNA ethidium bromide the decay time was 0.334 ms (Figure 15.29).

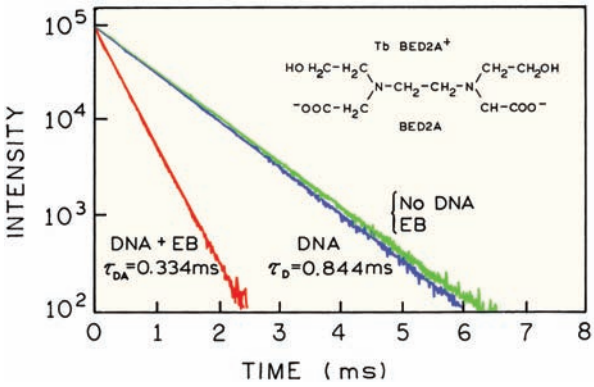

Figure 15.29. Intensity decays of TbBED2A$^+$ in the presence of DNA, or DNA with ethidium bromide (EB). The concentration of EB was 2.77 μM. Revised from [62].

For a donor in an infinite cylinder like DNA the diffusion limited transfer rate is given by

$$k_T^b = \frac{1.672R_0^6}{\tau_D r_C^3} \quad (\text{in } M^{-1}\text{sec}^{-1}) \qquad (15.25)$$

Calculate the observed value of k_T^b, and compare it with the maximum theoretical value assuming R_0 = 30.2 Å = 3.02 nm and r_c = 1.1 nm due to the combined radii of the donor and DNA. Explain the difference between the values of k_T^b.

P15.3. *Acceptor Concentrations for 50% Energy Transfer in One, Two, and Three Dimensions*: The equations describing the intensity decays in one, two, and three dimensions (eqs. 15.12, 15.9, and 15.1) were numerically integrated over time to obtain the relative donor quantum yields versus normalized concentrations (C/C_0). Using this graph (Figure 15.30) calculate the acceptor concentration for 50% transfer in a homogeneous solution (mM), for a mem-

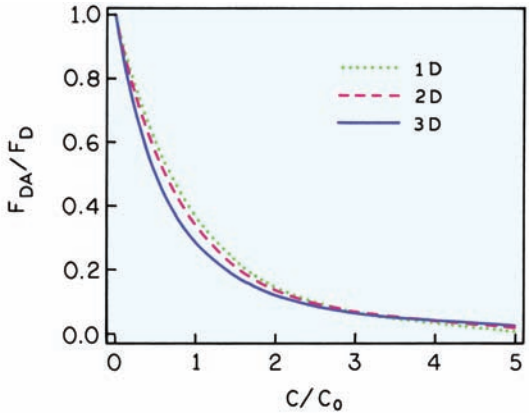

Figure 15.30. Relative donor quantum yield versus C/C_0 in one (1D), two (2D), and three (3D) dimensions.

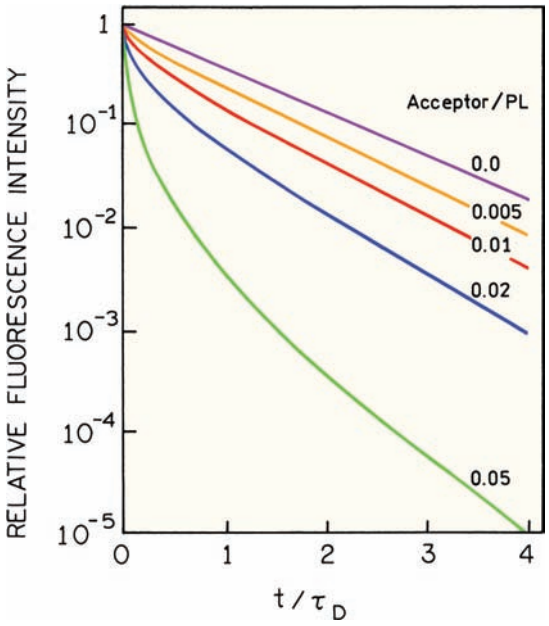

Figure 15.31. Calculated time-resolved decays of donor fluorescence for membrane-bound donors and acceptors. The area per lipid (PL) molecule was taken as 70 Å^2 per lipid. Revised from [50].

brane (acceptor per phospholipid), and for DNA (acceptor per base pair). For the membranes assume 70 Å^2 per phospholipid, and for DNA assume 3.4 Å per base pair. Use R_0 = 50 Å. Are these acceptor concentrations practical for proteins, membranes or nucleic acids?

P15.4. *Calculation of R_0 from the Extent of Donor Quenching*: Figure 15.31 shows calculated donor decays for membrane-bound donors and acceptors.[50] The simulations were performed using 70 Å^2 per lipid molecule and the acceptor densities (A/PL) shown in Figure 15.31. Calculate the R_0 value for this donor–acceptor pair.